



HAL
open science

Structure and sum-frequency generation spectra of water on uncharged Q 4 silica surfaces: a molecular dynamics study

Konstantin Smirnov

► **To cite this version:**

Konstantin Smirnov. Structure and sum-frequency generation spectra of water on uncharged Q 4 silica surfaces: a molecular dynamics study. *Physical Chemistry Chemical Physics*, 2020, 22 (4), pp.2033-2045. 10.1039/C9CP05765J . hal-02459452

HAL Id: hal-02459452

<https://hal.science/hal-02459452v1>

Submitted on 17 Nov 2020

HAL is a multi-disciplinary open access archive for the deposit and dissemination of scientific research documents, whether they are published or not. The documents may come from teaching and research institutions in France or abroad, or from public or private research centers.

L'archive ouverte pluridisciplinaire **HAL**, est destinée au dépôt et à la diffusion de documents scientifiques de niveau recherche, publiés ou non, émanant des établissements d'enseignement et de recherche français ou étrangers, des laboratoires publics ou privés.

Structure and sum-frequency generation spectra of water on hydrophobic and hydrophilic silica surfaces: a molecular dynamics study[†]

Konstantin S. Smirnov*

Univ. Lille, CNRS, UMR 8516 – LASIR – Laboratoire de Spectrochimie Infrarouge et Raman, F-59000 Lille, France

Structural characteristics and sum-frequency generation (SFG) spectra of water near hydrophobic and hydrophilic neutral silica surfaces were investigated by molecular dynamics simulations. Interactions of water molecules with atoms of the solid were described by different potential models, in particular by the CLAYFF [Cygan *et al.*, *J. Phys. Chem. B*, 2004, **108**, 1255] and INTERFACE [Heinz *et al.*, *Langmuir*, 2013, **29**, 1754] force fields. The calculations of the contact angle of water have shown that the silica surface modeled with CLAYFF behaves macroscopically hydrophilic, in contrast to the surface described with the INTERFACE model. The hydrophilicity of CLAYFF stems from too attractive electrostatic surface–water interactions. Regardless the surface’s affinity for water, the aqueous phase has a layered structure in the direction perpendicular to the surface with density fluctuations decaying within a distance of 10 Å from the surface. The orientational ordering of H₂O molecules was found to be more short-ranged than the density fluctuations, especially for the hydrophobic surfaces. Modeling the SFG spectra has shown that the spectra of all studied hydrophobic silica–water interfaces are similar and have features common with the spectrum of water–vapor interface. The spectra fairly agree with experimental results obtained for silica–water interface at low pH conditions [Myalitsin *et al.*, *J. Phys. Chem. C*, 2016, **120**, 9357]. The spectral response for the hydrophobic interface was computed to primarily arise from the topmost molecules of the first layer of interfacial water. In contrast, the SFG signal from the hydrophilic silica–water interface is accumulated over a greater distance extending for several water layers due to a more long-ranged perturbation of structure by the surface.

1 Introduction

Aqueous interfaces are ubiquitous in nature and are central to many fundamental processes and technological applications. Unraveling microscopic-level details of mechanisms driving the interfacial phenomena is paramount for numerous areas such as biochemistry, catalysis, corrosion, tribology, electrochemistry, *etc.*^{1,2} Interactions between water and mineral surfaces play a crucial role in the heterogeneous chemistry of atmosphere and geochemistry. Water present on the mineral surfaces may promote selective adsorption and sequestration of molecules, affect transport phenomena and drive the state of adsorbed species.^{3,4} Silicates, and silica in particular, are the most abundant minerals on Earth and the technological importance of silicon dioxide can hardly be overestimated. The understanding of interactions of water with silica surfaces is of significant importance from both the fundamental and application viewpoints. Although all silica surfaces consist of common structural units such as silanol groups (Si–OH) and siloxane bridges (Si–O–Si),^{5,6} the existence of a large number of silica polymorphs (dense, microporous, amorphous) makes it difficult to construct an unified model of silica–water interface and calls forth an unceasing research on the subject.

Among different experimental techniques employed in studying interfaces,⁷ information on the structure and dynamics at the atomic level is commonly obtained by means of vibrational spectroscopy. However, conventional spectroscopic techniques are not surface-specific and/or often incompatible with "wet" chemistry. The limitations can be circumvented with the use of the sum-frequency generation (SFG) vibrational spectroscopy that offers a valuable information on interfacial phenomena.⁸ The surface-specificity of the technique stems from the fact that the SFG response arises from the second-order nonlinear susceptibility $\chi^{(2)}$ which is nonzero at interfaces because of the broken inversion symmetry. While first SFG

*E-mail: konstantin.smirnov@univ-lille.fr

[†]Electronic Supplementary Information (ESI) available. Dipole and polarizability models, details on computation of nonlinear susceptibility, structural characteristics and SFG spectra of silica–water and water–vapor interfaces.

studies mainly concerned liquid-vapor interfaces,^{9,10} the method has been subsequently applied to the investigations of water on mineral surfaces,^{2,11} in particular on surfaces of silica and silica glasses.¹²⁻²⁹

The first study of silica-water system by the SFG spectroscopy reported on the fused quartz-water interface.¹² The authors observed two peaks in the SFG spectra and assigned them to interfacial regions with liquid-like and ice-like water structures. Changes seen in the spectra as a function of pH value of bulk water were ascribed to an order-disorder-order transition in a response to the change of surface charge due to the pH variation. In a subsequent study of crystalline quartz-water interface with the help of a phase-sensitive SFG setup, Shen and co-workers¹⁴ found that the orientation of water molecules in the ice-like and liquid-like regions responded differently to the pH change and explained the finding by the heterogeneity of sites on the surface. However, the origin of the two-peak feature in the spectrum of the system was recently contested by Myalitsin *et al.*¹⁸. The authors investigated an isotopically diluted water on a silica surface with heterodyne-detected SFG spectroscopy and concluded that the two peaks observed in the spectra of silica-water systems¹²⁻¹⁴ originate from the intramolecular and intermolecular vibrational coupling, but not from two distinct water structures; the dependence of the SFG spectra on pH value was explained by different orientations of the interfacial water molecules.

Although a variation of pH changes the nature of surface sites because of the protonation/deprotonation of surface OH groups, the surface of silica remains macroscopically hydrophilic. Nevertheless, some SFG studies provided evidence of hydrophobicity of silica surface at the molecular level. Thus, Isaenko and Bourguet¹⁶ studied water adsorbed on a flat surface of amorphous silica under ambient conditions with different relative humidity. A spectral feature attributed to isolated surface OH groups was found to be largely insensitive to the relative humidity that indicated, in authors' opinion, a hydrophobic character of the hydroxylated amorphous silica. This conclusion was, however, put in doubt in the work of Dalstein and co-workers.²³ Very recently, Cyran *et al.*²⁹ investigated a silica-water interface by a combination of macroscopic and microscopic techniques assisted by atomistic simulations. The authors identified a spectral signature of weakly bound OH groups belonging to water molecules adsorbed on a formally hydrophilic silica surface. The simulations showed that these OH groups bind to oxygen atoms of siloxane bridges that is in line with the results of ref. 16.

Spectral manifestations of hydrophobic/hydrophilic interactions on solid surfaces were investigated in refs. 30,31. Tyrode and Liljeblad³⁰ probed water structure next to a silica surface hydrophobized by silane monolayers. For highly ordered monolayers, water in the immediate proximity to the surface was found to behave similarly to the water-vapor interface with an SFG response only slightly modified by van der Waals interactions between the molecules and the substrate. The surface induced order in the water structure was obtained to be limited to a few angstroms and water recovered its bulk properties already at a sub-nanometer distance. Sanders and Petersen³¹ observed that the chemical nature of surface of self-assembled monolayers affects the interfacial water orientation. For a mixed hydrophilic/hydrophobic monolayer, the measured SFG spectrum resembled that of the hydrophilic surface, whereas the macroscopic characteristics, such as the contact angle, were similar to those of water adsorbed on the pure hydrophobic surface. The authors concluded that the macroscopic properties and the behaviour of surface at the atomic level may come from different surface parts.

Due to the complexity of fundamental mechanisms responsible for the SFG response and the heterogeneity of interfacial region, the interpretation of experimental SFG spectroscopic results necessitates the use of theoretical models and atomistic simulations.³²⁻³⁵ Like in experiments, much of effort in modeling studies has been concentrated on aqueous interfaces,³² while water adjacent to solid surfaces has received notably less attention. Structure and nonlinear spectra of water on some mineral surfaces were investigated by both classical and DFT-based molecular dynamics simulations³⁶⁻⁴³ Most of these computational studies dealt with OH-covered and/or charged surfaces whose behaviour is conditioned by the presence of strong adsorption sites. Modeling hydrophobic/hydrophilic interactions on neutral surfaces and their manifestations in the SFG spectra are less frequent.

The effect of surface hydrophobicity/hydrophilicity on the structure and phase behavior of water con-

finned between silica plates has been investigated in a series of works by Debenedetti and Rossky,^{44–47} but the spectroscopic issues were not addressed. Gaigeot *et al.*^{48,49} modeled characteristics of water on silica surface and related computed structural features to the two-band feature observed in the SFG spectra of the system.^{12–14} Recently, Joutsuka and co-workers⁴¹ conducted an MD study of nonlinear spectra of water on quartz surface. The authors succeeded to separate the contribution of the third-order susceptibility from the intrinsic SFG spectra of charged silica–water interface and obtained an SFG spectrum of a neutral quartz–water interface in a qualitative agreement with that measured by Myalitsin *et al.*¹⁸ for a low pH conditions. Manifestations of hydrophobic/hydrophilic interactions on a solid–water interface were investigated by Roy and Hore⁵⁰. The structure and spectral response of water near a hydrophobic surface mimicked by a methyl-terminated self-assembled monolayer were found to be similar to those of the water–vapor interface, in an agreement with the results by Tyrode and Liljeblad.³⁰ The study showed that a hydrophilic hydroxyl-terminated surface induced water ordering at a greater distance from the surface and the computed SFG spectrum resulted from a greater depth of interfacial water layer.

The present work reports results of molecular dynamics simulations of structural characteristics and sum-frequency generation vibrational spectra of water near hydrophobic and hydrophilic silica surfaces. The main aims of the study were (i) to investigate the structure of water layer near silica surfaces of different affinity for the molecules and the spatial extent of structural perturbations induced by the surfaces, and (ii) to unveil how the specific structural organization of the interfacial region manifests itself in the sum-frequency generation vibrational spectrum. The modeled surface is neutral, OH-free and consists of siloxane bridges that are known to be hydrophobic.⁵¹ The silica–water interactions were described with two potential models, CLAYFF by Cygan and co-workers⁵² and the INTERFACE force field by Heinz *et al.*⁵³ and an additional insight into the influence of potential model on the system behaviour was obtained by modifying the surface’s hydrophobicity by varying values of silica charges in the CLAYFF force field.

2 Models and computations

2.1 Structural and potential models

2.1.1 Silica surface.

Model of silica surface was extracted from the surface model database for silica by Emami *et al.*⁵⁴ and it is a Q₄ silica model obtained from the α -cristobalite structure cut parallel to the (20 $\bar{2}$) plane; the surface contains no silanol groups, it is neutral and corresponds to pH \sim 2 – 4.⁵⁴ Such a surface is characteristic of silica substrates annealed at a high temperature. Except when mentioned explicitly, the layer used in the calculations has dimensions of 25.026 Å and 24.885 Å in the xy plane (surface plane) and a thickness of 21.93 Å in the z direction perpendicular to the surface.⁵⁵ The model contains 360 silicon and 720 oxygen atoms. The positions of atoms of the layer were kept fixed in the simulations.

2.1.2 Water slab.

Water molecules were represented with the SPCFw water model⁵⁶ with a slightly modified intramolecular part (*vide infra*). A water slab was obtained in an MD simulation of 500 SPCFw molecules in a slab geometry with dimensions of the MD box in the x and y directions equal to those of the silica layer; the resulting slab thickness⁵⁵ was equal to *ca.* 24 Å. The simulation was run in an NVT ensemble at 293 K for 200 ps.

2.1.3 Silica–water interface.

The so-obtained slab of water molecules was inserted between two surfaces of the silica layer; the system layout is shown in Figure 1. The initial distance between the silica surfaces was set to the thickness of the water slab plus van der Waals diameter of the SPC oxygen atom. For each system studied, the interlayer distance was varied till the zz component of stress tensor computed in a 200 ps NVT MD run became less than its root mean squared fluctuation. The resulting structure was subsequently used as an initial configuration in a series of production runs (*vide infra*).

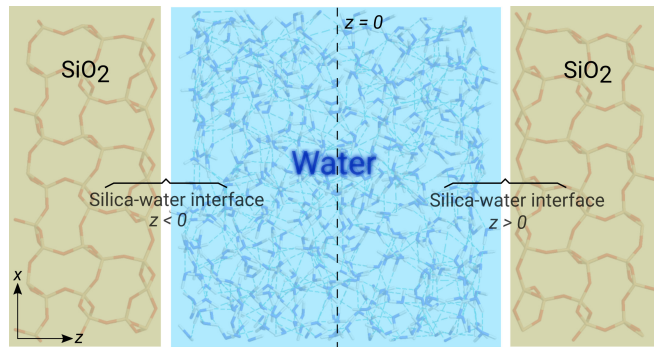


Figure 1: A layout of system used in the study.

2.1.4 Interaction potentials.

The energy of nonbonded interatomic interactions E_{NB} was described by the sum of Lennard-Jones (12-6) and Coulomb potentials

$$E_{NB} = \sum_i \sum_j D_{0,ij} \left[\left(\frac{R_{0,ij}}{r_{ij}} \right)^{12} - 2 \left(\frac{R_{0,ij}}{r_{ij}} \right)^6 \right] + \frac{q_i q_j}{r_{ij}}, \quad (1)$$

where the indices i and j run over atoms, D_0 and R_0 are the Lennard-Jones potential energy minimum and the corresponding interatomic distance, respectively, and q denotes atomic charge. Parameters D_0 and R_0 for pairs of unlike atoms were computed by the Lorentz-Berthelot combination rules.

Four sets of D_0 , R_0 and q parameters were employed for water-silica interaction potentials. First three sets used parameters of the CLAYFF force field⁵² for van der Waals interactions, but different values of silica atomic charges. The first set had charges equal to zero, charges of the second set were computed with a split-charge equilibration method calibrated on the electrostatic potential (ESP),⁵⁷ while the third set employed authentic CLAYFF charges.⁵² In what follows, these three sets are referred to as QNULL, QESP and CLAYFF, respectively. The fourth set is the INTERFACE force field proposed by Heinz and co-workers.^{53,54,58} Table 1 gathers values of the parameters in the four sets.

Table 1: Values of parameters^a of eqn. (1) in different sets.

Atom ^b	QNULL, QESP, CLAYFF					INTERFACE		
	R_0	D_0	q^c	q^d	q^e	R_0	D_0	q
Si	3.7064	$1.8405 \cdot 10^{-6}$	0.00	1.38	2.10	4.150	0.093	1.10
O	3.5532	0.155	0.00	-0.69	-1.05	3.470	0.054	-0.55

^a R_0 in Å, D_0 in kcal/mol, q in $|e|$. ^b Si - tetrahedral silicon, O - two-coordinated bridging oxygen. ^c QNULL set, ^d QESP set, ^e CLAYFF set.

The energy of intramolecular interactions E_B in a water molecule was modeled with a combination of Morse potential for the OH bond-stretchings, a harmonic angle-bending potential for the HOH angle and harmonic cross terms for the interaction between the internal coordinates

$$E_B = \sum_{i=1}^2 D_e \left[e^{-2\gamma\Delta r_i} - 2e^{-\gamma\Delta r_i} \right] + \frac{1}{2} K_\theta \Delta\theta^2 + K_{rr} \Delta r_1 \Delta r_2 + \sum_{i=1}^2 K_{r\theta} \Delta r_i \Delta\theta. \quad (2)$$

In (2), the index i runs over the OH bonds of molecule, r and θ stands for the length of OH bond and the HOH angle, respectively, and Δ denotes a deviation from the equilibrium value. The equilibrium geometry of water molecule corresponded to the SPCFw model.⁵⁶ Parameters D_e , γ , K_θ , K_{rr} and $K_{r\theta}$ were

fitted to reproduce the experimental frequencies of the vibrational modes of a free water molecule and the anharmonicity constant of OH bond. Values of the parameters are reported in Table 2.

Table 2: Parameters of intramolecular potential energy functions (2) of SPCFw water molecule.

D_e (kcal/mol)	γ (\AA^{-1})	K_θ (mdyn $\cdot\text{\AA}$)	K_{rr} (mdyn/ \AA)	$K_{r\theta}$ (mdyn)
115.658	2.1866	0.727	-0.016	0.260

2.2 Property calculations

2.2.1 Surface characterization.

The affinity of surface for water at the microscopic level was quantified by computing the water-surface interaction energy obtained in a series of MD runs performed for a single water molecule adsorbed on the surface. The calculations were carried out for temperatures of 293 K and 100 K in an NVT ensemble. The sum of MD trajectory lengths was equal to 4 ns.

The hydrophilic/hydrophobic behaviour of surface at the macroscopic level is commonly characterized by the contact angle. To calculate the angle, a set of 864 SPCFw water molecules (a cube with 29.45 \AA side) taken from a bulk water simulation was placed on the surface of silica layer with dimensions of $75.078 \times 74.655 \text{\AA}$ in the directions parallel to the surface.⁵⁹ For each set of parameters, the initial structure was equilibrated for 500 ps at $T = 293 \text{ K}$ and the equilibration stage was followed by an 1 ns production run during which the coordinates of atoms were saved each 0.5 ps for a subsequent analysis. The simulations were carried out in an NVT statistical ensemble. The shape of the water droplet was analyzed by computing the radial water density profile $\rho(r, z) = \langle N_{rz} \rangle / V_r$, where V_r is the volume of a 3D ring with radii r and $r + \Delta r$ and of thickness Δz , and $\langle N_{rz} \rangle$ is the mean number of water molecules in the ring at the distance z from the surface; Δr and Δz were equal to 0.5 \AA and 1 \AA , respectively. The z -axis origin corresponded to the z -coordinate of the topmost silica oxygen atom and the xy frame origin was placed in the CoM of the droplet. The droplet radius for each z was defined as a distance r at which the density $\rho(r, z)$ decreased to ρ_0/e with $\rho_0 = 0.0334 \text{\AA}^{-3}$ being the number density of bulk SPCFw water. The contact angle was then computed using the shape of the droplet in the rz coordinates as discussed in Section 3.1.2.

2.2.2 Structure of silica-water interface.

Structure of interlayer water was characterized by a profile of relative water density $\rho(z)^* = \rho(z)/\rho_0$ in the direction z perpendicular to the surface and by two-dimensional probability density maps of molecular CoMs in the xy plane. Orientations of molecules as a function of z distance from the surface were assessed by computing profiles of orientational order parameter $S_2(z)$

$$S_2(z) = \left\langle \frac{1}{N_z} \sum_{i=1}^{N_z} P_2(\cos \varphi_i) \right\rangle, \quad (3)$$

where φ_i stands for the angle between either the dipole μ or HH vector of molecule i and the z -axis, N_z is the number of molecules in a slice from z to $z + \Delta z$ and $P_2()$ is the second Legendre polynomial; the angle brackets in (3) denote averaging over trajectory. $S_2(z) = -0.5$ corresponds to a mean vector orientation perpendicular to the z -axis, $S_2(z) = 1$ indicates the vector orientation parallel to the axis, while $S_2(z) = 0$ points to the absence of orientational ordering. The Δz value in the z -profile calculations was equal to 0.05 \AA . Additional insights into the structure of interfacial water was obtained from radial distribution functions and probability density maps for angles between the OH bond vectors and the z -axis.

2.2.3 Sum-frequency vibrational spectra.

The intensity of the radiation emitted at the sum of frequencies of the visible and IR light and measured by the SFG spectroscopy is proportional to the square of the second-order nonlinear susceptibility tensor

$\chi^{(2)}$.^{8,35,60} The tensor is the sum of the resonant (R) and non-resonant (NR) parts

$$\chi^{(2)} = \chi^{(2),R} + \chi^{(2),NR}, \quad (4)$$

where $\chi^{(2),NR}$ gives a real frequency-independent contribution to $\chi^{(2)}$ in electronically off-resonance conditions. By virtue of the symmetry at interfaces, only seven elements of the third-rank $\chi^{(2)}$ tensor are not equal to zero.^{8,61} A common attention is paid to $\chi_{ssp}^{(2)}$ element that is probed with s - and p polarized visible and IR pulses, respectively, and is detected with emitted SFG radiation in s -polarization. For the system shown in Figure 1 with the surface plane coinciding with the xy plane and the z -axis perpendicular to the surface, the ssp term corresponds to the average of the $\chi_{xxz}^{(2)}$ and $\chi_{yyz}^{(2)}$ elements due to the isotropy in the azimuthal angle. The following discussion focuses on the vibrationally resonant part of the second-order susceptibility tensor. The imaginary part of $\chi_{ssp}^{(2),R}$ can be measured in phase-sensitive (heterodyne-detected) SFG experiments and provides a direct information about the orientation of molecular adsorbates on surfaces.^{14,35,62}

The frequency-dependent $\chi^{(2),R}(\omega)$ tensor was computed using the time correlation function formalism.^{60,63,64} According to the approach, the pqr element of $\chi^{(2),R}(\omega)$ is given by

$$\chi_{pqr}^{(2),R}(\omega) = \frac{i\omega}{k_B T} \int_0^\infty dt e^{i\omega t} \langle M_r(0) \cdot A_{pq}(t) \rangle, \quad (5)$$

where M_r and A_{pq} stand for the r and pq components of the system dipole \mathbf{M} and polarizability \mathbf{A} , respectively, and k_B is the Boltzmann constant. Details on models for the dipole and polarizability and on the computation of the cross correlation function in (5) are given in ESI.[†]

The analysis of the characteristics discussed in Sections 2.2.2 and 2.2.3 exploited the symmetry of the system with respect to the xy plane with $z = 0$ (Fig. 1). For the sake of definiteness, the following discussion of results refers to a half space with the water slab lying beneath the silica surface and with the z -axis directed toward the surface; the z -coordinate of the bottommost surface oxygen atoms is taken as the origin of z -axis.

2.3 Molecular dynamics simulations

The classical equations of motion were integrated using the velocity form of Verlet algorithm with the integration time-step equal to 0.5 fs. The real space cut-off radius for the short-range and electrostatic interactions was equal to 10 Å. The cut-off radius is smaller than a half of the thickness of both the silica layer and water slab and consequently, H_2O molecules in the proximity to the surface cannot "see" each other through either solid or liquid phases. The discontinuity of the short-range energy and force at the cut-off distance was treated with a shifted-force technique. The long-range electrostatic interactions were handled using a damped shifted-force modification of Wolf method^{65,66} with a damping parameter of 0.2 Å⁻¹.⁶⁶ Temperature in NVT runs was controlled via a chain of Nosé-Hoover thermostats.

The MD simulations were performed for a target temperature of 293 K. A typical production run consisted of a 20 ps equilibration period in the NVT ensemble followed by 50 ps period in a microcanonical NVE ensemble. The positions and velocities of atoms were stored each 4 fs during the last 40 ps of the NVE stage. Reported results were obtained as an average of at least 50 MD runs (up to 200 runs were performed for computing the nonlinear spectra). In sampling the phase space, the last configuration of previous run was used as a starting configuration of the subsequent run while the atomic velocities in each simulation were newly chosen from the Maxwell-Boltzmann distribution at the target temperature. The MD simulations and analysis were performed with in-house programs.

3 Results and discussion

3.1 Surfaces characterization

3.1.1 Water-surface interaction energy.

Figure 2 displays distributions of the silica–water interaction energy (E_{SW}) computed with the different sets of parameters. The calculations with CLAYFF were performed for the temperature of 293 K, whereas frequent desorption events of H_2O molecule led to a large uncertainty of the energy in simulations with the three other sets at this target temperature. To limit the desorption, the simulations with the QNULL, QESP and INTERFACE sets were carried out at $T = 100$ K. The obtained mean values of the E_{SW} energy are equal to -2.4 (1.3) kJ/mol, -20.0 (1.9) kJ/mol, -29.2 (6.5) kJ/mol and -18.0 (2.6) kJ/mol for the QNULL, QESP, CLAYFF and INTERFACE surfaces, respectively. As these values are smaller in magnitude than the intermolecular interaction energy in the bulk liquid SPCFw water $E_{WW} = -40.8$ kJ/mol, all the four surfaces can be formally characterized as hydrophobic (Fig. 2). However, one can notice that the energy distribution in the case of the CLAYFF surface, extends slightly beyond the E_{WW} value, that has an important consequence for the macroscopic characteristics of water on this surface.

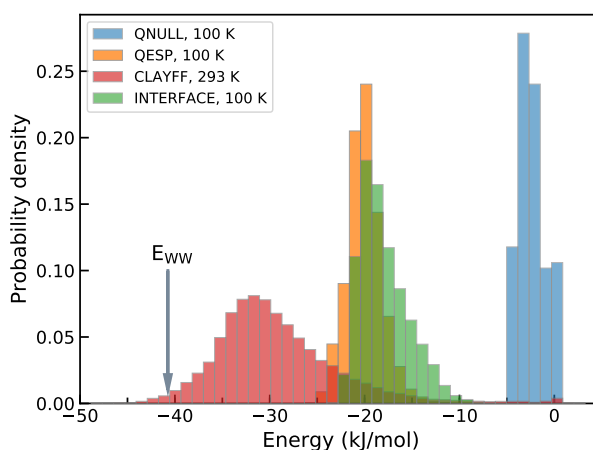


Figure 2: Distributions of the water-silica interaction energy E_{SW} computed with the QNULL, QESP, CLAYFF and INTERFACE parameter sets. The arrow indicates the interaction energy in bulk water E_{WW} .

3.1.2 Contact angle.

The shapes of the water droplet obtained in the contact angle calculations are shown in Figure 3 for the four surfaces. By fitting the droplet profile with the function $r(z) = az^2 + bz + c$ for $z > 3$ Å and $r > 15$ Å, the contact angle θ_c can be obtained as $\theta_c = \pi/2 + \arctan(dr(z)/dz|_{z=3})$.⁴⁵ The z offset of 3 Å excludes the density in the zone under the droplet that is irrelevant to the contact angle calculations; the uncertainty due to the choice of offset does not exceed 2° . The computed values of θ_c are equal to 128° , 99° , 46° and 103° for the QNULL, QESP, CLAYFF and INTERFACE surfaces, respectively. For water adsorbed on a graphite surface, Werder and co-workers⁶⁷ have shown that the contact angle decreases when the number of molecules in a water droplet increases. Consequently, given the relatively small number of molecules in the contact angle calculations ($\approx 10^3$), the θ_c values above should be considered as upper estimates.

Based on the values of the contact angle, one can qualify all but CLAYFF surface as hydrophobic. Interestingly, the latter surface behaves macroscopically hydrophilic despite the mean E_{SW} value smaller than the E_{WW} energy (Fig. 2). Anticipating results presented in Section 3.2.3, the hydrophilicity stems from the existence of relatively strong adsorption sites on the surface that manifest themselves as a high-energy tail in the E_{SW} energy distribution. Molecules diffused to these sites act as nucleation centers that leads to a progressive spreading of the droplet over the surface and results in the contact angle value typical of hydrophilic substrates. This outcome is in line with results of ref. 46, where small hydrophilic patches on a hydrophobic surface were found to strongly affect properties of the latter vis-à-vis water.

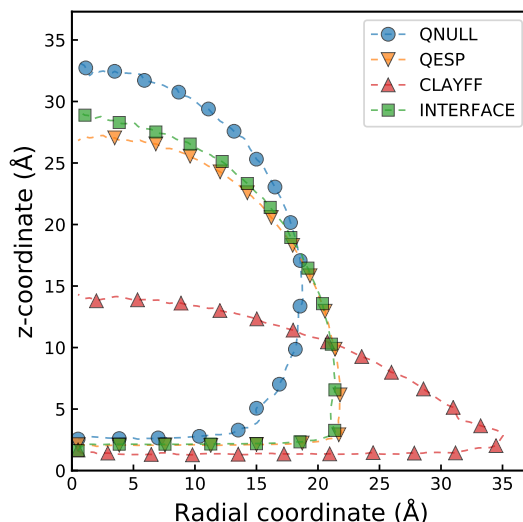


Figure 3: Shape of water droplet on silica surfaces computed with different sets of potential parameters. The limit of the radial coordinate corresponds to a half of the shortest MD box dimension in the surface plane.

The model silica surface studied in the present work consists of siloxane bridges and contains neither surface OH groups nor non-bridging oxygen atoms that could act as hydrophilic adsorption sites. As the siloxane bridges are known to be hydrophobic,⁵¹ the surface is expected to be hydrophobic too. This is indeed the case for the QNULL, QESP, INTERFACE surfaces, whereas the CLAYFF one has a hydrophilic character as revealed by the contact angle calculations. Too strong affinity of CLAYFF silica for water has already been mentioned. Thus, Ho *et al.*⁶⁸ found that the CLAYFF force field produced a more hydrophilic OH-covered silica surface compared to a surface described with a force field by Bródka and Zerda.⁶⁹ Although the contact angles computed with both potential models were smaller than 90° , the calculation of water density profiles perpendicular to the surface showed that the CLAYFF surface attract the molecules more strongly.

Since the difference between the QESP and CLAYFF sets is the values of atomic charges, the hydrophilic character of the CLAYFF surface apparently results from too strong electrostatic solid–water interactions. Grand canonical Monte Carlo simulations of water condensation in silicalite-1 (purely siliceous zeolite of MFI topology) have shown that the partial charge on Si atoms should be kept below $1.7 |e|$ in order to reproduce the experimental liquid-phase adsorption isotherm.⁷⁰ It is noteworthy that the Si charge in the Bródka and Zerda force field⁶⁹ is below this value and is close to the charge of the QESP set (Table 1). Probably, the ESP charges provide upper estimates of atomic charges that still make the neutral Q_4 silica surface macroscopically hydrophobic when using the Lennard-Jones parameters of the SPC water model for oxygen-oxygen interactions.

The subsequent sections of the paper, in the main, will limit the discussion to results obtained with two sets of parameters, namely CLAYFF and INTERFACE. These sets provide complete potential models for the atomistic simulations of silica-water systems while, according to the results presented above, they yield the Q_4 silica surface of quite different affinity for water molecules. Results calculated for the silica–water interface with the QNULL and QESP sets, if not discussed explicitly, are qualitatively similar to those obtained with the INTERFACE force field and the corresponding data are reported in ESI.[†]

3.2 Structural characteristics of silica-water interface

3.2.1 Radial distribution functions.

Figure 4 presents O_WO and H_WO radial distribution functions $g(r)$ computed with the four sets of parameters (the subscript W denotes atoms of water molecules). A main difference seen in the RDFs for the hydrophilic and hydrophobic surfaces is the intensity of the first peak. Thus, $g_{O_WO}(r)$ for the CLAYFF sur-

face has a clear peak at *ca.* 2.7 Å whereas such a peak is ill-defined in the case of the hydrophobic surfaces, Figure 4a. The H_WO RDF (Fig. 4b) has also markedly higher intensity of the first peak for the hydrophilic surface than for the hydrophobic ones. The $g(r)$ function computed with QNULL set is structureless that reflects the absence of directional surface–water interactions due to the zero charges of solid atoms in this set. One should notice the sensitivity of the peaks position to the charges of silica atoms (QNULL, QESP, CLAYFF sets) and Figure 4 clearly demonstrates the structuring character of the electrostatic interactions.

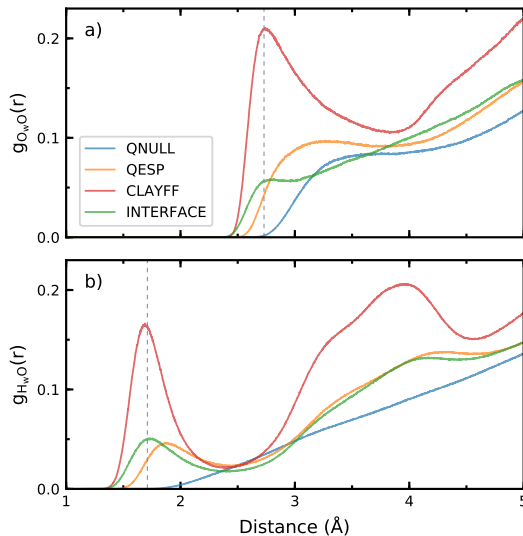


Figure 4: O_WO (a) and H_WO (b) radial distribution functions $g(r)$ computed for the water-silica system with the CLAYFF and INTERFACE sets; the subscript *W* denotes atoms of water molecules. Vertical dashed lines indicate the position of the first peak in the corresponding RDFs for bulk liquid water.

The higher intensity of the first peak in the RDFs for the hydrophilic surface indicates a higher probability of finding the involved pairs of atoms at the corresponding distance and points once more to that the CLAYFF surface attracts water molecules more strongly than the INTERFACE one (and other hydrophobic surfaces). On the other hand, the positions of the first peaks in the RDFs computed with the CLAYFF and INTERFACE models are nearly the same and the corresponding interatomic distances are practically identical to those in bulk liquid water.

3.2.2 z-profiles.

Figure 5a,c display z -profiles of the relative water density ρ^* computed near the hydrophilic and hydrophobic surfaces. For all potential models used in the simulations, the density in the direction perpendicular to the surface has an oscillating behaviour and converges to $\rho^* = 1$ at a distance of *ca.* 10 Å from the surface. On the other hand, one can notice some important differences in the profiles shown in Figure 5a and Figure 5c. First, water density near the hydrophilic surface is significantly greater than near the hydrophobic one with the difference in the maximum ρ^* values of about 30 %. Second, while the first peak in $\rho^*(z)$ for the hydrophobic INTERFACE surface features a shoulder from the large z side, the peak for the CLAYFF surface has a complex structure with two sub-peaks and a shoulder at small z -values. Third, the first minimum in $\rho^*(z)$ is found at 3.02 Å for the hydrophilic surface compared to 4.82 Å for the hydrophobic INTERFACE surface. Finally, the density oscillations near the hydrophilic surface are characterized by a smaller period and decay less rapidly. The arrow symbolized by z_1 and the allied vertical dotted line in Figure 5 denote an interfacial region, hereafter named z_1 , corresponding to the first surface water layer defined by the z -coordinate of the first minimum in $\rho^*(z)$.

The z -profiles of the orientational order parameter (3) for the molecular dipole and for the HH vector computed with the CLAYFF and INTERFACE sets are presented in Figure 5b,d. The comparison of the profiles with the density fluctuations in Fig. 5a,c shows that the orientational ordering is more short-ranged. Like in the case of the density, the z -profiles of the S_2 order parameters for water near the hydrophilic

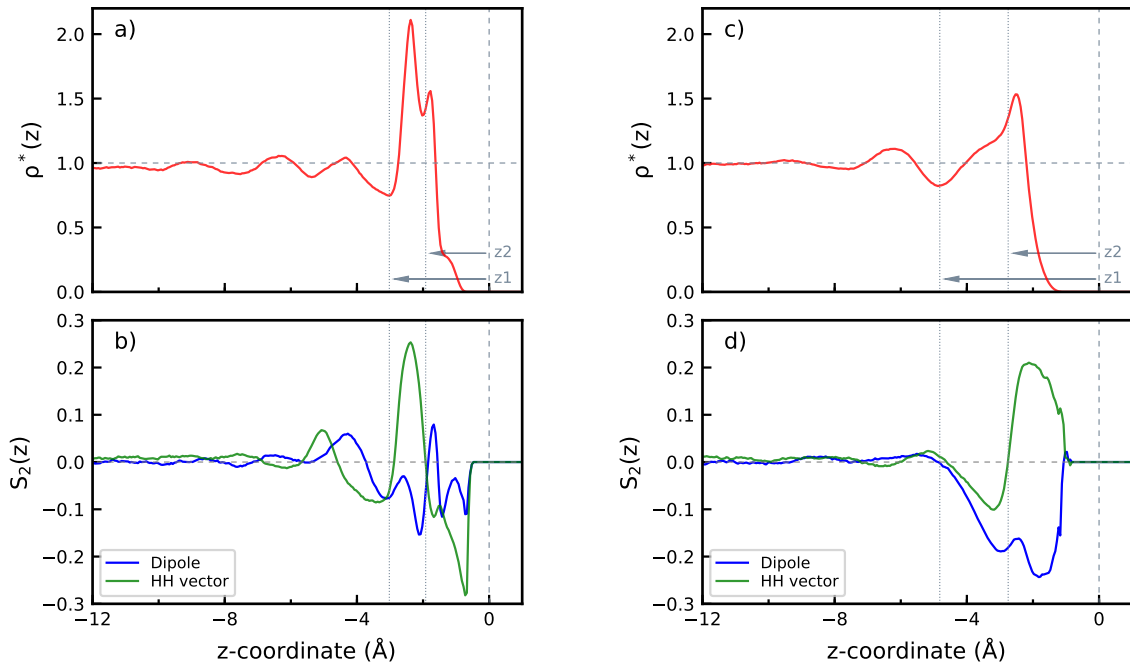


Figure 5: z -profiles of the relative density $\rho^* = \rho/\rho_0$ and of the orientational order parameters $S_2(z)$ of water molecules near the CLAYFF surface (panels a, b) and INTERFACE surface (panels c, d). The vertical dashed line at $z = 0$ denotes the coordinate of the bottommost silica oxygen atoms taken as the origin of the z -axis; the horizontal dashed line indicates property value characteristic of bulk liquid water. The vertical dotted lines and the corresponding arrows labeled z_1 and z_2 are discussed in the text.

CLAYFF surface have a more complex shape, Figure 5b. One can notice that oscillations of the parameters extend up to the third water layer (*cf.* Fig. 5a). The HH vector S_2 parameter changes its sign twice within the z_1 region near the CLAYFF surface. The first change of the sign occurs close to the z_1 distance and then, the parameter changes its sign the second time at *ca.* 2 \AA from the surface. This z coordinate defines a region marked by the second vertical dotted line in Figure 5a, indicated with the arrow z_2 and referred to as z_2 region below. Note that the z_2 coordinate nearly matches the minimum between the two density sub-peaks in the z_1 region, *cf.* Figure 5a. By analyzing the z -profile of the HH vector order parameter, one can infer that a preferred orientation of the vector is parallel to the z -axis in the region $z_1 < z < z_2$, whereas the orientation turns into a perpendicular one in the zone $z > z_2$. Similar analysis of the dipole S_2 parameter indicates that the dipole has a tendency to a perpendicular-to-surface orientation within the first water layer, but a complex profile of $S_2(z)$ hampers a more detailed analysis. Assuming that the magnitude of the order parameter reflects the degree of orientation ordering, Figure 5b clearly shows a more ordered structure of water in the $z_1 < z < z_2$ region.

For the hydrophobic INTERFACE surface, both the S_2 parameters (Fig. 5d) rapidly decay to zero beyond the first water layer (*cf.* Fig. 5c). The dipole parameter has negative values within the first layer, while the $S_2(z)$ parameter for the HH vector changes its sign from negative (far from the surface) to positive (close to the surface). The distance at which the change of the sign occurs is marked by the second vertical dotted line in Figure 5c and denotes the corresponding z_2 region. Negative values of the dipole S_2 parameter in the water layer next to the hydrophobic surface suggest that the molecules tend to orient their dipoles perpendicular to the z -axis. On the other hand, the HH vector S_2 parameter changing its sign indicates the existence of two different average orientations of the vector in the z_1 region. Molecules in the zone $z_1 < z < z_2$ have slightly negative S_2 values corresponding to a preferred orientation of the HH vector perpendicular to the z -axis. Molecules with $z > z_2$ are characterized by a positive S_2 parameter and they tend to align their HH vectors parallel to the z -axis. The magnitude of the order parameter in Figure 5d indicates a more ordered structure of water in the z_2 region. It is worthy of note that both

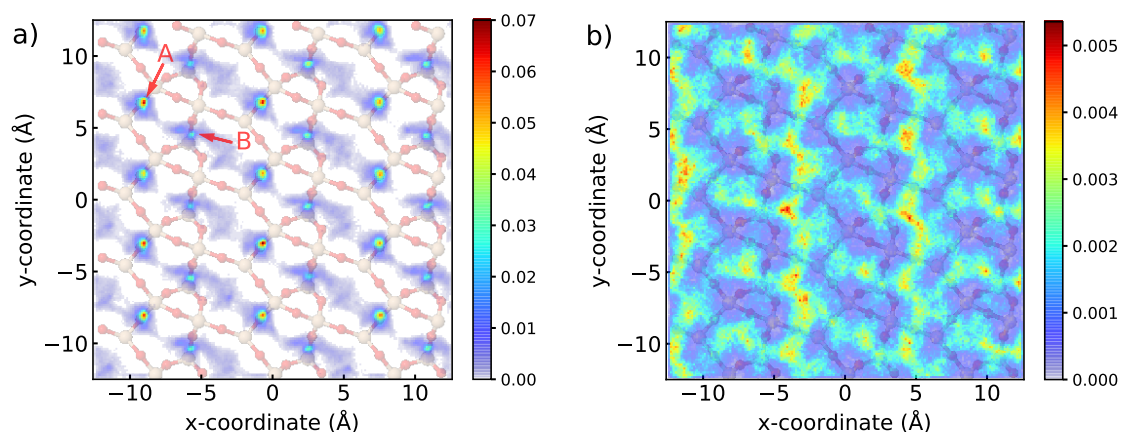


Figure 6: Maps of probability density (in \AA^{-2}) for water molecules in the plane parallel to the surface in the z_2 region; a) – CLAYFF surface, b) – INTERFACE surface. Structure of the silica surface is shown as a background (silicons – peach, oxygens – red).

the S_2 parameters behave qualitatively similar for all hydrophobic surfaces studied in the work and their behaviour resembles that for water–vapor interface, see Figure S5 and Figure S10 of ESI.[†]

3.2.3 Water density in the surface plane.

The structure of water layer near the surfaces can further be analyzed by using the distributions of water in the plane parallel to the surface (xy plane). Figure 6 shows such probability density maps computed for molecules in the z_2 region near the CLAYFF and INTERFACE surfaces. One can readily notice a localized character of water adsorption on the CLAYFF surface and the analysis of Figure 6a points to the presence of two adsorption sites indicated by arrows and labeled A and B in the figure. Taking the probability density value as a measure of water–surface interaction strength, Figure 6 suggests that molecules interact stronger with the sites A than with the sites B. Both these sites are already detectable in the map for the QNULL surface and they gradually increase in strength, although to a different extent, with increasing the silica charges.[†] Certainly, these adsorption sites are at the origin of the hydrophilic character of the CLAYFF surface and molecules localized in these sites account for the density features in the z_2 region in Figure 5d. Inspection of configurations of molecules in the z_2 region reveals that the molecules adsorbed in the site A are coordinated by their oxygens to two silicon atoms and prefer to point their hydrogens to the liquid phase, Figure 7. Orientations of molecules in the site B is less apparent, but one of the hydrogens of the molecule tends to be directed toward the surface, as shown in Figure 7.

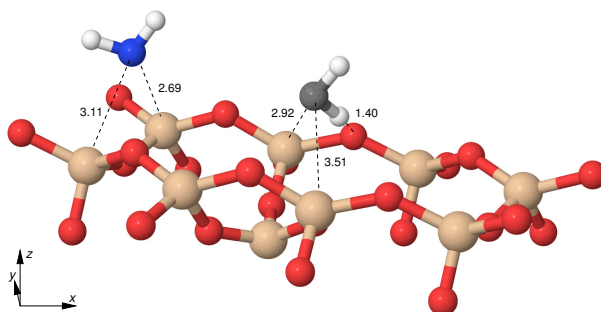


Figure 7: A fragment of snapshot showing water molecules adsorbed in the sites A and B. Atom colors: hydrogens – white, silica oxygens – red, silicon – peach, oxygen of water in site A – blue, oxygen of water in site B – grey. Digits indicate the lengths (in \AA) of the interatomic contacts shown with dashed lines.

In contrast, the probability density map for molecules in the z_2 region near the hydrophobic surface (Fig. 6b) shows a more uniform distribution of water molecules in the xy plane. Despite a certain templating effect by the surface on the water distribution, no well defined adsorption sites can be distinguished

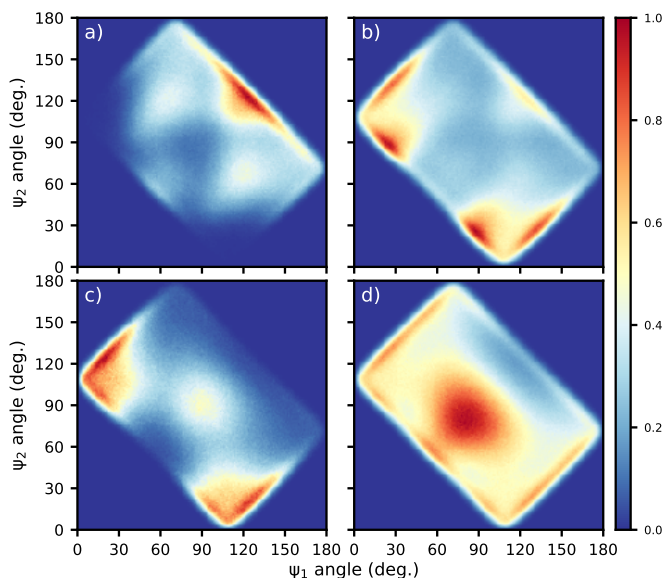


Figure 8: Two-dimensional probability density maps (in arb. units) of the angles ψ between the OH bonds and the z -axis for water molecules near the CLAYFF (a, b) and INTERFACE (c, d) surfaces. Panels a, c – region z_2 ; panels b, d – region z_1 , see Fig. 5.

in Figure 6b. It is worthy of noting that regions with a high probability density on the INTERFACE surface do not match the adsorption sites on the CLAYFF one. In particular, the sites A seem to be excluded, presumably because of a large van der Waals diameter of silicon atoms in the INTERFACE force field (see Table 1).

3.2.4 OH bonds orientation.

Figure 8 displays two-dimensional maps of probability density for angles ψ_1 and ψ_2 defined as angles between the OH bond vectors of water molecule and the z -axis, Figure 9. The zone covered on the maps is defined by the HOH equilibrium angle value and the permutation symmetry of bond indices (maps are symmetrical with respect to the $\psi_2 = \psi_1$ line). One sees that the maps computed for the hydrophilic and hydrophobic surfaces have very different patterns. The most probable orientation of the water molecules in the z_2 region near the hydrophilic CLAYFF surface is characterized by the ψ angles of about 120° that corresponds to both the OH bonds pointing away from the surface, see configuration I in Figure 9. Comparing Figure 8a and Figure 6a, one can attribute this orientation to molecules adsorbed in the site A, Figure 7. One can also notice in this z region the presence of a second type of molecules with an orientation $(\psi_1, \psi_2) \approx (60^\circ, 120^\circ)$ that can probably be ascribed to molecules in the site B. Further from the surface one finds molecules with most probable orientations with $(\psi_1, \psi_2) \approx (25^\circ, 90^\circ)$ and $(\psi_1, \psi_2) \approx (25^\circ, 130^\circ)$, Figure 8b. Molecules with these orientations have one of OH bonds directed toward the surface, whereas the second bond points to the liquid phase ($\psi_2 \approx 130^\circ$) or is parallel to the surface ($\psi_2 \approx 90^\circ$), as sketched with configurations II in Figure 9. Note that the majority of molecules in the first water layer near the hydrophilic surface has these orientations.

Contrarily, water molecules in the immediate proximity to the hydrophobic INTERFACE surface tend to direct one of OH bonds toward the surface ($\psi_1 < 30^\circ$), whereas the second bond points to the liquid phase ($\psi_2 > 90^\circ$), Figure 8c. These orientations are similar to those found for molecules in the $z_1 < z < z_2$ region near the hydrophilic surface and they account for the sign of the S_2 parameters in the z_2 region near the INTERFACE surface. However, the most probable orientations of molecules in the first layer near the surface are characterized by the ψ angles distributed around 90° , *i.e.* the molecules tend to lie in a plane parallel to the surface, Figure 8d. These orientations can explain the negative values of the S_2 order parameters in the $z_1 < z < z_2$ region near the surface (Fig. 5d) and they are depicted with the configuration III in Figure 9.

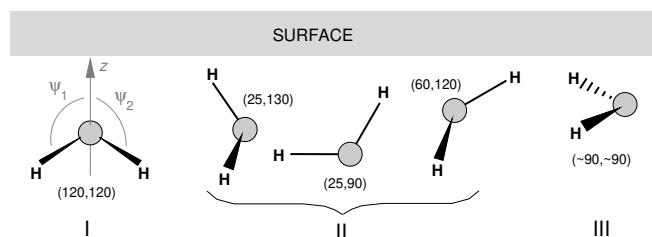


Figure 9: A sketch of different orientations of water molecules near the hydrophobic and hydrophilic surfaces. Digits in the parenthesis refer to the pairs of ψ_1, ψ_2 angles discussed in the text.

The results presented above concerning the structure of interfacial water on the hydrophobic and hydrophilic Q_4 silica surfaces can be summarized as follows. Regardless the surface affinity for water, the solid–water interface is characterized by an oscillating behaviour of water density in the direction perpendicular to the surface with the density of the interfacial water converging to the bulk value at a distance less than 10 \AA from both the surfaces. A stronger interaction of molecules with the hydrophilic surface leads to a more compact water structure with the first surface layer that can be twice as dense as the bulk liquid water (Fig. 5a). The orientational ordering of water molecules near surfaces is more short-ranged than the density fluctuations. In particular, the ordering near the hydrophobic surface does not extend beyond the water layer next to the surface with the topmost molecules having a preferential orientation with one OH bond directed toward the surface and the second one pointing to the liquid phase. This structural organization is also characteristic of other hydrophobic surfaces studied in the work.[†] In contrast, the hydrophilic surface perturbs an orientational ordering of water at a greater distance that spans more than one water layer. In general, the structural organization of water near the hydrophilic surface is found to be more complex and is governed by a localized adsorption on surface sites that are responsible for the surface hydrophilicity. Consequently, both the structure of adsorbed water layer and the orientational ordering of molecules near hydrophilic surfaces are likely to be dependent on the surface chemistry and/or topography.

These results are in line with experimental data and the outcome of previous modeling studies. Thus, the layered structure of interfacial water was observed experimentally for oxide surfaces^{71,72} and obtained in simulations of solid–water interface.^{45–47,67,68,73,74} Vibrational SFG spectroscopy studies of water on hydrophobic surfaces commonly indicated the presence of molecules with one OH bond (free OH bonds) directed toward the surface.^{30,75–77} Tyrode and Liljeblad³⁰ found that the water structure on the surface of well-ordered hydrophobic monolayers is not much affected beyond the first surface layer. Furthermore, the present simulations agrees with the results by Roy and Hore⁵⁰ who pointed to a more complicated behaviour of density and order parameters of water in contact with a hydrophilic surface than near a hydrophobic one. These authors also mentioned that the structure of water close the hydrophilic surface is perturbed to a greater distance.

3.3 Sum-frequency generation spectra

Figure 10 displays $\text{Im}[\chi_{ssp}^{(2),R}]$ spectra computed for water near the INTERFACE and CLAYFF surfaces⁷⁸ and compares them with the corresponding spectrum of water–vapor (WV) interface.[†] The latter is perhaps the most studied aqueous interface, both experimentally^{76,79} and theoretically,^{32,60,80} with a firm interpretation of features in the sum-frequency generation vibrational spectrum. According to the interpretation, the positive high-frequency and negative low-frequency peaks in the spectrum are attributed to the stretching vibrations of free and hydrogen-bonded OH bonds of interfacial water molecules, respectively. Due to different values of the OH force constants, the bond-stretching vibrations are energetically uncoupled and the directions of the vibrational transition dipole moments almost coincide with the O–H vectors. For the free OH bond pointing into the vapor phase, the transition dipole moment has a positive cosine with the z -axis, whereas for the bond involved in the H-bonding and directed toward the liquid phase, the transition

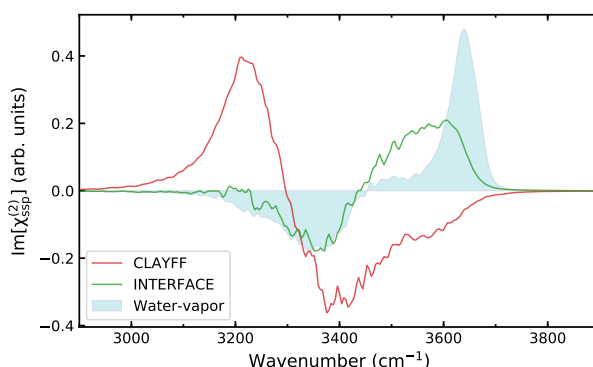


Figure 10: Spectrum of $\text{Im}[\chi_{ssp}^{(2),R}]$ for the CLAYFF and INTERFACE silica–water interfaces; the spectrum for water–vapor interface is given for comparison as a filled shape.

dipole moment has a negative value of the cosine. These signs are just reflected in the signs of the spectral features and the spectrum thereby yields a direct information about the orientation of H_2O molecules at the interface.

Figure 10 shows that the spectrum of water near the hydrophobic INTERFACE surface has much in common with the spectrum of the WV interface with the difference that the high-frequency positive peak in the spectrum is shifted to lower wavenumbers and has a larger width. The interpretation of the spectral features is essentially the same as for the water–vapor interface, while the red shift and broadening of the positive high-frequency band can be explained by interactions between the "free" OH bonds and the surface atoms. The calculated spectrum is in line with the experimental spectra of water on hydrophobic substrates such as surfaces of self-assembled monolayers⁷⁷ and hydrophobically modified silica³⁰. Computational studies of water/liquid⁸¹ and water/solid^{50,82} hydrophobic interfaces also revealed the spectral response of interfacial water similar to the SFG spectrum of water–vapor interface. The downward shift of the high-frequency OH peak relative its position in the WV spectrum was found to be dependent on the nature of hydrophobic media and on the strength of water–substrate interactions.^{77,81,82}

The calculated spectrum favourably compares with the spectrum of silica–water interface at low pH, when the SiO_2 surface is neutral. Using the heterodyne-detected SFG setup, Myalitsin *et al.*¹⁸ identified two water species in the interfacial region of the system. Weakly bonded molecules were obtained to have an H-up orientation by donating H-bond to the oxygen atoms of siloxane bridges or to silanol groups, whereas molecules forming stronger bonds with the surrounding orient their H atoms away from the surface. Consequently, the measured $\text{Im}[\chi_{ssp}^{(2)}]$ spectrum had a negative low-frequency band and a positive high-frequency band, both characterized by a large width. A recent combined experimental and computational study by Cyran *et al.*²⁹ provided strong evidence that the observed high-frequency positive feature is indeed due to H-up water molecules adsorbed on hydrophobic sites of silica surface. The calculated shift of the high-frequency band with respect to its position in the spectrum of WV interface is equal to 40 cm^{-1} that well agrees with the value of 36 cm^{-1} obtained in the experiments.²⁹

Figure 10 shows that the $\text{Im}[\chi_{ssp}^{(2),R}]$ spectrum of water near the hydrophilic CLAYFF surface is very different from the spectrum of water on the hydrophobic silica. The low- and high-frequency bands in the spectrum reverse their signs suggesting that the most strongly perturbed OH oscillators are now directed toward the surface, whereas the less perturbed OH bonds point to the liquid phase. This peculiarity of the SFG spectrum can arguably be explained by strong water–surface interactions that prevail the intermolecular ones because of a large negative charge of CLAYFF oxygen ($q_{\text{O}} = -1.05 |e|$, Table 1). The molecular orientation deduced from the computed spectrum corresponds to the configurations of type II in Figure 9 and the two-dimensional map in Figure 8b indeed reveals that molecules with such orientations are abundant in the first water layer near the surface. It is noteworthy that the simulated spectrum resembles the experimental spectrum of silica/water interface at high pH, when the surface is deprotonated and has

Si–O[−] entities acting as strong H-bond acceptors.^{18,24}

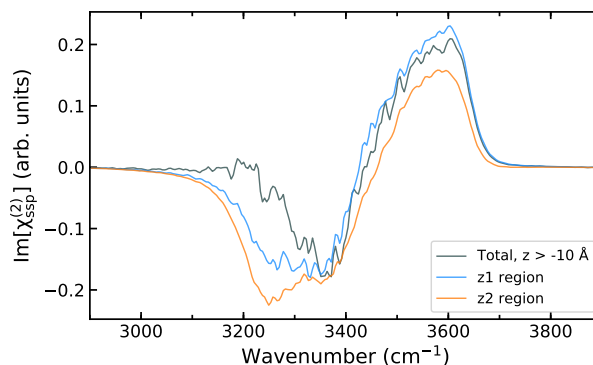


Figure 11: Spectrum of $\text{Im}[\chi_{ssp}^{(2),R}]$ as a function of the distance z from the INTERFACE surface, see Figure 5.

Analysis of the SFG spectra as a function of distance from the surface provides additional insights into the origin of the SFG spectral response. Figure 11 displays the $\text{Im}[\chi_{ssp}^{(2),R}]$ spectra of water on the hydrophobic INTERFACE surface computed for different accumulation depths.⁸³ The high-frequency positive feature in the spectra shows a relatively weak dependence on the layer thickness. Such a behaviour is consistent with the attribution of the band to the "free" OH oscillators of molecules in the $z2$ region. This is also in line with the fact that molecules with z -coordinates $z1$ to $z2$ tend to lie parallel to the surface (see Fig. 8d) and therefore, they give a minor contribution to the ssp spectrum. On the other hand, the spectrum below 3400 cm^{-1} reveals a notable variation of intensity with the increase of accumulation depth. Thus, increasing the layer thickness leads to fading the band at 3250 cm^{-1} . This result suggests the OH oscillators of this energy effectively cancel each other out in the entire water slab. This finding indicates that the lack of spectral intensity does not necessarily mean the lack of oscillators of this energy, but can be caused by a cancellation effect.⁵⁰ One may conclude, although with a certain degree of caution, that the SFG signal of water near a hydrophobic surface primarily comes from the topmost molecules of the first water layer. Corresponding results for the QNULL and QESP hydrophobic surfaces is given in ESI.[†]

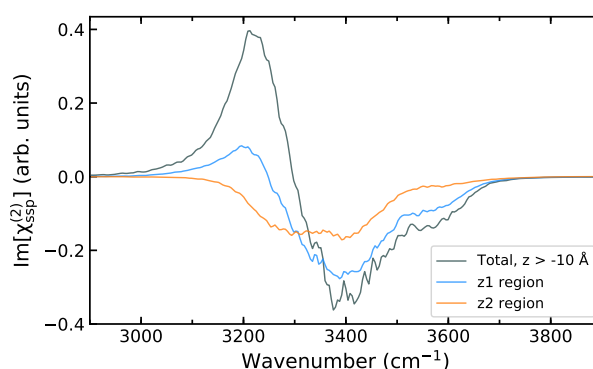


Figure 12: Spectrum of $\text{Im}[\chi_{ssp}^{(2),R}]$ as a function of the distance z from the CLAYFF surface, see Figure 5.

Figure 12 shows the spectra of the hydrophilic CLAYFF interface computed for the different z depths. One sees that the spectrum for the $z2$ region is markedly different from the spectrum of the $z1$ region and of that for the entire water slab. Indeed, the $z2$ -region spectrum is characterized by the negative intensity for all wavenumbers that agrees with orientations of molecules with the two OH bonds directed away from the surface, as revealed by Figure 7 and the analysis of Figure 8a. The spectrum of the topmost water molecules in the first layer can be set against SFG spectra of the CaF_2 /water system at low pH values that features a negative intensity due to H-down oriented water molecules near a positively charged fluorite surface.^{37,84–86} A recent computational study of water on an anatase TiO_2 surface has also shown such

a negative peak in the SFG spectrum that originated from water coordinated to surface Ti atoms via its oxygen and donated H-bonds to molecules of the liquid phase.⁴⁰

As it follows from Figure 8b, the majority of water molecules in the first water layer have orientations with one H atom pointing toward the surface (configurations II in Fig. 9). Consequently, the spectrum of the z1 region features a positive peak of low intensity at 3200 cm^{-1} while the H-down oriented bonds of the molecules account for the increase of the negative intensity at 3400 cm^{-1} . Further increase of intensity of the positive and negative bands in the spectrum of the entire water slab (Fig. 12) shows that the SFG spectral response of water near the hydrophilic surface is accumulated over a z-region which is not limited to the first surface layer, in contrast to the hydrophobic surfaces. This result is in line with the fact that the orientational ordering of water near the hydrophilic surface extends over several water layers.

4 Conclusions

The present work reports results of computational study of the structural characteristics and nonlinear spectra of water near hydrophobic and hydrophilic neutral Q_4 silica surfaces. The silica–water interaction were represented by two potential models, namely the CLAYFF⁵² and INTERFACE⁵³ force fields. In addition, the influence of force field parameters on the behaviour of interfacial water was examined by varying the values of silica charges of the CLAYFF model.

Results of the calculations show that the CLAYFF and INTERFACE models yield hydrophilic and hydrophobic silica surfaces, respectively. Although the mean values of the water-surface interaction energies calculated with the models are smaller than the intermolecular energy in bulk liquid water, the CLAYFF surface behaves macroscopically hydrophilic, as revealed by the contact angle value of $\theta_c = 46^\circ$ (2°) compared to $\theta_c = 103^\circ$ (2°) computed for the hydrophobic INTERFACE surface. This peculiarity results from the existence of strong adsorption sites on the CLAYFF surface. The flaw of CLAYFF in mimicking the hydrophobicity of neutral OH-free silica surface is ascribed to a large magnitude of charges on silica atoms in the model. The deficiency is, perhaps, not critical for studying water on intrinsically hydrophilic, e.g. hydroxyl-covered, surfaces, although a certain overstructuring of the interfacial region caused by too attractive surface–water interactions can be expected.⁶⁸

In agreement with the experimental results and data of previous computational studies, the interfacial water near the surfaces has a layered structure. The density fluctuations decay at approximately the same distance from the surfaces of both types so that the density reaches its bulk value at a depth of about 10 \AA . The hydrophilic surface was obtained to induce a more dense first layer of surface water than the hydrophobic surface does. The calculation of the orientational order parameters for the molecular dipole and the HH vector shows that the orientation of molecules is perturbed by the surfaces at lesser distances than the density. Thus, the surface-induced orientational ordering does not extend beyond the first surface layer near the hydrophobic surfaces; for the hydrophilic surface the perturbation of molecular orientations is more long-ranged.

Modeling the sum-frequency generation spectra of the systems shows that the spectra of hydrophobic surface–water interfaces are similar to each other and they have much in common with the spectrum of water–vapor interface. The simulated spectra fairly agree with the experimental spectra of silica–water interface at low pH values.¹⁸ The analysis of the depth dependence of the calculated spectra indicate that the SFG response of water on the hydrophobic surface mainly results from water molecules of the first water layer. Contrarily, as the hydrophilic surface perturbs molecular orientations at a greater distance, the SFG response for the system is accumulated over several water layers so that the total signal can mask the SFG spectrum characteristic of molecules next to the surface. The calculated SFG spectrum of water on the hydrophilic CLAYFF surface was obtained to differ from the experimental spectra of neutral silica-water interface because of the above mentioned deficiency of the force field. The structural organization of water near a hydrophilic silica surface and, consequently the SFG spectrum of such interface, are likely to be dependent on the surface chemistry and topography and work is in progress to elucidate the issue.

Conflicts of interest

There are no conflicts to declare.

Notes and references

- [1] M. A. Henderson, *Surf. Sci. Rep.*, 2002, **46**, 1–308.
- [2] O. Björneholm, M. H. Hansen, A. Hodgson, L.-M. Liu, D. T. Limmer, A. Michaelides, P. Pedevilla, J. Rossmeisl, H. Shen, G. Tocci, E. Tyrode, M.-M. Walz, J. Werner and H. Bluhm, *Chem. Rev.*, 2016, **116**, 7698–7726.
- [3] W. Stumm, L. Sigg and B. Sulzberger, *Chemistry of the solid-water interface : processes at the mineral-water and particle-water interface in natural systems*, John Wiley & Sons, New York, 1992.
- [4] A. M. Jubb, W. Hua and H. C. Allen, *Acc. Chem. Res.*, 2012, **45**, 110–119.
- [5] *Characterization and Chemical Modification of the Silica Surface*, ed. E. Vansant, P. V. D. Voort and K. Vrancken, Elsevier, 1995, vol. 93, pp. 59 – 77.
- [6] L. Zhuravlev, *Colloid. Surface. A*, 2000, **173**, 1–38.
- [7] F. Zaera, *Chem. Rev.*, 2012, **112**, 2920–2986.
- [8] Y. R. Shen, *Fundamentals of Sum-Frequency Spectroscopy*, Cambridge University Press, University Printing House, Cambridge CB28BS, UK, 2016, p. 316.
- [9] R. Superfine, J. Y. Huang and Y. R. Shen, *Phys. Rev. Lett.*, 1991, **66**, 1066–1069.
- [10] Q. Du, R. Superfine, E. Freysz and Y. R. Shen, *Phys. Rev. Lett.*, 1993, **70**, 2313–2316.
- [11] P. A. Covert and D. K. Hore, *Annu. Rev. Phys. Chem.*, 2016, **67**, 233–257.
- [12] Q. Du, E. Freysz and Y. R. Shen, *Phys. Rev. Lett.*, 1994, **72**, 238–241.
- [13] V. Ostroverkhov, G. A. Waychunas and Y. R. Shen, *Chem. Phys. Lett.*, 2004, **386**, 144 – 148.
- [14] V. Ostroverkhov, G. A. Waychunas and Y. R. Shen, *Phys. Rev. Lett.*, 2005, **94**, 046102.
- [15] L. Zhang, S. Singh, C. Tian, Y. R. Shen, Y. Wu, M. A. Shannon and C. J. Brinker, *J. Chem. Phys.*, 2009, **130**, 154702.
- [16] O. Isaienko and E. Borguet, *Langmuir*, 2013, **29**, 7885–7895.
- [17] S. Dewan, M. S. Yeganeh and E. Borguet, *J. Phys. Chem. Lett.*, 2013, **4**, 1977–1982.
- [18] A. Myalitsin, S.-h. Urashima, S. Nihonyanagi, S. Yamaguchi and T. Tahara, *J. Phys. Chem. C*, 2016, **120**, 9357–9363.
- [19] J. Luo, J. Banerjee, C. G. Pantano and S. H. Kim, *Langmuir*, 2016, **32**, 6035–6045.
- [20] A. J. Souna, T. L. Clark and J. T. Fourkas, *J. Phys. Chem. C*, 2017, **121**, 26432–26437.
- [21] J. Schaefer, G. Gonella, M. Bonn and E. H. G. Backus, *Phys. Chem. Chem. Phys.*, 2017, **19**, 16875–16880.
- [22] K. A. Lovering, A. K. Bertram and K. C. Chou, *J. Phys. Chem. Lett.*, 2017, **8**, 871–875.
- [23] L. Dalstein, E. Potapova and E. Tyrode, *Phys. Chem. Chem. Phys.*, 2017, **19**, 10343–10349.
- [24] S.-h. Urashima, A. Myalitsin, S. Nihonyanagi and T. Tahara, *J. Phys. Chem. Lett.*, 2018, **9**, 4109–4114.
- [25] N. Sheth, D. Ngo, J. Banerjee, Y. Zhou, C. G. Pantano and S. H. Kim, *J. Phys. Chem. C*, 2018, **122**, 17792–17801.
- [26] B. Rehl, Z. Li and J. M. Gibbs, *Langmuir*, 2018, **34**, 4445–4454.
- [27] B. Rehl, M. Rashwan, E. L. DeWalt-Kerian, T. A. Jarisz, A. M. Darlington, D. K. Hore and J. M. Gibbs, *J. Phys. Chem. C*, 2019, **123**, 10991–11000.
- [28] D. K. Hore and E. Tyrode, *J. Phys. Chem. C*, 2019, **123**, 16911–16920.
- [29] J. D. Cyran, M. A. Donovan, D. Vollmer, F. Siro Brigiano, S. Pezzotti, D. R. Galimberti, M.-P. Gaigeot, M. Bonn and E. H. G. Backus, *Proc. Natl. Acad. Sci.*, 2019, **116**, 1520–1525.

- [30] E. Tyrode and J. F. D. Liljeblad, *J. Phys. Chem. C*, 2013, **117**, 1780–1790.
- [31] S. E. Sanders and P. B. Petersen, *J. Chem. Phys.*, 2019, **150**, 204708.
- [32] T. Ishiyama, T. Imamura and A. Morita, *Chem. Rev.*, 2014, **114**, 8447–8470.
- [33] S. A. Hall, K. C. Jena, P. A. Covert, S. Roy, T. G. Trudeau and D. K. Hore, *J. Phys. Chem. B*, 2014, **118**, 5617–5636.
- [34] T. Ishiyama and A. Morita, *Ann. Rev. Phys. Chem.*, 2017, **68**, 355–377.
- [35] A. Morita, *Theory of Sum Frequency Generation Spectroscopy*, Springer, Singapore, 2018, vol. 97.
- [36] S.-Y. Ma, L.-M. Liu and S.-Q. Wang, *J. Phys. Chem. C*, 2016, **120**, 5398–5409.
- [37] R. Khatib, E. H. G. Backus, M. Bonn, M.-J. Perez-Haro, M.-P. Gaigeot and M. Sulpizi, *Sci. Rep.*, 2016, **6**, 24287.
- [38] M. DelloStritto and J. Sofo, *J. Phys. Chem. A*, 2017, **121**, 3045–3055.
- [39] G. Melani, Y. Nagata, J. Wirth and P. Saalfrank, *J. Chem. Phys.*, 2018, **149**, 014707.
- [40] M. F. Calegari Andrade, H.-Y. Ko, R. Car and A. Selloni, *J. Phys. Chem. Lett.*, 2018, **9**, 6716–6721.
- [41] T. Joutsuka, T. Hirano, M. Sprik and A. Morita, *Phys. Chem. Chem. Phys.*, 2018, **20**, 3040–3053.
- [42] F. Creazzo, D. R. Galimberti, S. Pezzotti and M.-P. Gaigeot, *J. Chem. Phys.*, 2019, **150**, 041721.
- [43] S.-H. Chen and S. J. Singer, *J. Phys. Chem. B*, 2019, **123**, 6364–6384.
- [44] N. Giovambattista, P. J. Rossky and P. G. Debenedetti, *Phys. Rev. E*, 2006, **73**, 041604.
- [45] N. Giovambattista, P. G. Debenedetti and P. J. Rossky, *J. Phys. Chem. B*, 2007, **111**, 9581–9587.
- [46] N. Giovambattista, P. G. Debenedetti and P. J. Rossky, *J. Phys. Chem. C*, 2007, **111**, 1323–1332.
- [47] N. Giovambattista, P. J. Rossky and P. G. Debenedetti, *J. Phys. Chem. B*, 2009, **113**, 13723–13734.
- [48] M.-P. Gaigeot, M. Sprik and M. Sulpizi, *J. Phys.: Condens. Matter*, 2012, **24**, 124106/1–124106/11.
- [49] M. Sulpizi, M.-P. Gaigeot and M. Sprik, *J. Chem. Theory Comput.*, 2012, **8**, 1037–1047.
- [50] S. Roy and D. K. Hore, *J. Phys. Chem. C*, 2012, **116**, 22867–22877.
- [51] J. Laskowski and J. A. Kitchener, *J. Colloid Interface Sci.*, 1969, **29**, 670–679.
- [52] R. T. Cygan, J.-J. Liang and A. G. Kalinichev, *J. Phys. Chem. B*, 2004, **108**, 1255–1266.
- [53] H. Heinz, T.-J. Lin, R. Kishore Mishra and F. S. Emami, *Langmuir*, 2013, **29**, 1754–1765.
- [54] F. S. Emami, V. Puddu, R. J. Berry, V. Varshney, S. V. Patwardhan, C. C. Perry and H. Heinz, *Chem. Mater.*, 2014, **26**, 2647–2658.
- [55] The layer thickness is defined as the difference of z -coordinates of the topmost and lowermost oxygen atoms.
- [56] Y. Wu, H. L. Tepper and G. A. Voth, *J. Chem. Phys.*, 2006, **124**, 024503.
- [57] T. Verstraelen, S. V. Sukhomlinov, V. Van Speybroeck, M. Waroquier and K. S. Smirnov, *J. Phys. Chem. C*, 2012, **116**, 490–504.
- [58] The INTERFACE force field has parameters for the (12-6) or (9-6) functional forms of van der Waals interactions. This work uses parameters for the (12-6) potential.
- [59] The silica layer is a $3 \times 3 \times 1$ layer described in Section 2.1.1. The size of the water droplet was chosen to be smaller than a half of the smallest MD box dimension in the xy plane; the initial cubic shape of the droplet is destroyed during a first few picoseconds of the equilibration stage of the simulation.
- [60] A. Morita and J. T. Hynes, *J. Phys. Chem. B*, 2002, **106**, 673–685.
- [61] A. G. Lambert, P. B. Davies and D. J. Neivandt, *Appl. Spectrosc. Rev.*, 2005, **40**, 103–145.
- [62] Y. R. Shen, *Annu. Rev. Phys. Chem.*, 2013, **64**, 129–150.
- [63] A. Perry, H. Ahlborn, B. Space and P. B. Moore, *J. Chem. Phys.*, 2003, **118**, 8411–8419.

- [64] A. Perry, C. Neipert, C. R. Kasprzyk, T. Green, B. Space and P. B. Moore, *J. Chem. Phys.*, 2005, **123**, 144705.
- [65] D. Wolf, P. Keblinski, S. R. Phillpot and J. Eggebrecht, *J. Chem. Phys.*, 1999, **110**, 8254–8282.
- [66] C. J. Fennell and J. D. Gezelter, *J. Chem. Phys.*, 2006, **124**, 234104.
- [67] T. Werder, J. H. Walther, R. L. Jaffe, T. Halicioglu and P. Koumoutsakos, *J. Phys. Chem. B*, 2003, **107**, 1345–1352.
- [68] D. Ho, Tuan A. and Argyris, D. V. Papavassiliou, A. Striolo, L. L. Lee and D. R. Cole, *Mol. Simul.*, 2011, **37**, 172–195.
- [69] A. Bródka and T. W. Zerda, *J. Chem. Phys.*, 1996, **104**, 6319–6326.
- [70] N. Desbiens, A. Boutin and I. Demachy, *J. Phys. Chem. B*, 2005, **109**, 24071–24076.
- [71] L. Cheng, P. Fenter, K. L. Nagy, M. L. Schlegel and N. C. Sturchio, *Phys. Rev. Lett.*, 2001, **87**, 156103.
- [72] J. G. Catalano, P. Fenter and C. Park, *Geochim. Cosmochim. Acta*, 2007, **71**, 5313–5324.
- [73] K. S. Smirnov, *Phys. Chem. Chem. Phys.*, 2017, **19**, 2950–2960.
- [74] J. Wang, A. G. Kalinichev and R. J. Kirkpatrick, *J. Phys. Chem. C*, 2009, **113**, 11077–11085.
- [75] L. F. Scatena, M. G. Brown and G. L. Richmond, *Science*, 2001, **292**, 908–912.
- [76] G. L. Richmond, *Chem. Rev.*, 2002, **102**, 2693–2724.
- [77] A. J. Hopkins, C. L. McFearnin and G. L. Richmond, *J. Phys. Chem. C*, 2011, **115**, 11192–11203.
- [78] The spectra were obtained with the parameters $z_0 = 9.5 \text{ \AA}$ and $s = 2.2 \text{ \AA}^{-1}$ (1 \AA transition region), eqn. S23[†].
- [79] M. Bonn, Y. Nagata and E. H. G. Backus, *Angew. Chem. Int. Ed.*, 2015, **54**, 5560–5576.
- [80] A. Morita and J. T. Hynes, *Chem. Phys.*, 2000, **258**, 371–390.
- [81] T. Ishiyama, Y. Sato and A. Morita, *J. Phys. Chem. C*, 2012, **116**, 21439–21446.
- [82] T. Ohto, H. Tada and Y. Nagata, *Phys. Chem. Chem. Phys.*, 2018, **20**, 12979–12985.
- [83] The spectra for the z_1 and z_2 regions were computed with $z_0 = z_1$ and $z_0 = z_2$, respectively, and with the parameter $s = 8.8 \text{ \AA}^{-1}$ (0.25 \AA transition region), eqn. S23[†].
- [84] K. A. Becraft and G. L. Richmond, *Langmuir*, 2001, **17**, 7721–7724.
- [85] K. A. Becraft, F. G. Moore and G. L. Richmond, *J. Phys. Chem. B*, 2003, **107**, 3675–3678.
- [86] N. Takeshita, M. Okuno and T.-a. Ishibashi, *J. Phys. Chem. C*, 2017, **121**, 25206–25214.

Electronic Supplementary Information

Structure and sum-frequency generation spectra of water on hydrophobic and hydrophilic silica surfaces: a molecular dynamics study

Konstantin S. Smirnov*

Univ. Lille, CNRS, UMR 8516 – LASIR – Laboratoire de Spectrochimie Infrarouge et Raman, F-59000 Lille, France

1 Dipole and polarizability models

1.1 Dipole and polarizability of water slab

The dipole \mathbf{M} and polarizability \mathbf{A} of a system of water molecules were obtained as the sum of corresponding molecular quantities

$$\mathbf{M} = \sum_i \boldsymbol{\mu}_i \quad (\text{S1})$$

$$\mathbf{A} = \sum_i \mathbf{a}_i \quad (\text{S2})$$

with $\boldsymbol{\mu}_i$ and \mathbf{a}_i denoting the dipole moment and polarizability tensor of molecule i , respectively. The effect of intermolecular interactions in condensed phase was taken into account with dipole interaction model.^{1,2} In a system of N interacting molecules that are characterized by permanent dipoles $\boldsymbol{\mu}^0$ and polarizability tensors $\boldsymbol{\alpha}$, the dipole $\boldsymbol{\mu}_i$ of molecule i is given by

$$\boldsymbol{\mu}_i = \boldsymbol{\mu}_i^0 + \boldsymbol{\alpha}_i (\boldsymbol{\mathcal{E}}_i^0 + \sum_{j \neq i} \hat{T}_{ij} \boldsymbol{\mu}_j), \quad (\text{S3})$$

where $\boldsymbol{\mathcal{E}}_i^0$ is an external electric field at the molecule's position \mathbf{r}_i and \hat{T}_{ij} is the dipole-dipole interaction tensor

$$\hat{T}_{ij} = \frac{1}{r_{ij}^3} (3\mathbf{e}_{ij}\mathbf{e}_{ij}^T - \mathbf{1}) \quad (\text{S4})$$

with $\mathbf{e}_{ij} = \mathbf{r}_{ij}/r_{ij}$ ($\mathbf{r}_{ij} = \mathbf{r}_i - \mathbf{r}_j$) and $\mathbf{1}$ being an unit matrix. The set of N equations (S3) can be rewritten in a matrix form

$$\mathbf{m} = \mathbf{m}^0 + \mathbf{a}(\mathbf{E}^0 + \mathbf{T}\mathbf{m}) = \mathbf{m}^0 + \mathbf{a}\mathbf{E}, \quad (\text{S5})$$

where $\mathbf{E} = \mathbf{E}^0 + \mathbf{T}\mathbf{m}$. The formal solution of (S5) for \mathbf{E} reads

$$\mathbf{E} = (\mathbf{1} - \mathbf{T}\mathbf{a})^{-1} (\mathbf{E}^0 + \mathbf{T}\mathbf{m}_0) \quad (\text{S6})$$

and therefore, one obtains the vector of dipoles \mathbf{m} as

$$\mathbf{m} = \mathbf{m}^0 + \mathbf{a}(\mathbf{1} - \mathbf{T}\mathbf{a})^{-1} (\mathbf{E}^0 + \mathbf{T}\mathbf{m}_0) = \mathbf{m}^0 + \mathbf{a}^{\text{eff}}(\mathbf{E}^0 + \mathbf{T}\mathbf{m}_0), \quad (\text{S7})$$

*E-mail: konstantin.smirnov@univ-lille.fr

where $\mathbf{a}^{\text{eff}} \equiv \mathbf{a}(\mathbf{1} - \mathbf{Ta})^{-1}$ is a $3N \times 3N$ matrix of effective system polarizability. The dipole $\boldsymbol{\mu}_i$ of molecule i is readily available from (S7), whereas the polarizability tensor \mathbf{a}_i is given by²

$$\mathbf{a}_i = \sum_j \mathbf{a}_{ij}^{\text{eff}}, \quad (\text{S8})$$

where the sum runs over 3×3 blocks of the matrix \mathbf{a}^{eff} .

1.2 Dipole and polarizability models for water molecule

The dipole $\boldsymbol{\mu}_i^0$ and polarizability $\boldsymbol{\alpha}_i$ of an isolated water molecule were obtained with models based on those proposed by Morita and Hynes².

Dipole model. Dipole of a molecule is computed as

$$\boldsymbol{\mu}^0 = \sum_k q_k \mathbf{r}_k \quad (\text{S9})$$

where q_k and \mathbf{r}_k denote the charge and position vector of atom k , respectively. In order to reproduce changes of $\boldsymbol{\mu}^0$ upon the dynamics of atoms, the atomic charges q_k were made geometry-dependent. Following ref. 2, the variation charge Δq_i of each of the two hydrogen atoms ($i = 1, 2$) is written in the form

$$\Delta q_i \equiv q_i - q_{\text{H}}^0 = a\Delta R_i + b\Delta R_i^2 + c\Delta\theta + d\Delta\theta^2 + e\Delta R_i\Delta R_j + f\Delta R_i\Delta\theta, \quad (\text{S10})$$

where q_{H}^0 is the charge in the equilibrium geometry, ΔR and θ are deviations of OH bond length and HOH angle θ from their equilibrium values, respectively, and a, b, c, d, e, f are coefficients.

By using symmetry-adapted internal coordinates

$$S_1 = \Delta R_1 + \Delta R_2, \quad S_2 = \Delta R_1 - \Delta R_2 \quad \text{and} \quad S_3 = \Delta\theta \quad (\text{S11})$$

to describe variations of molecular geometry, one can obtain the following expressions for symmetry-adapted variations of Δq_i

$$\Delta q_1 + \Delta q_2 = C_1 S_1 + C_2 S_1^2 + C_3 S_2^2 + C_4 S_3 + C_5 S_3^2 + C_6 S_1 S_3 \quad (\text{S12})$$

$$\Delta q_1 - \Delta q_2 = C_7 S_2 + C_8 S_1 S_2 + C_9 S_2 S_3 \quad (\text{S13})$$

$$\Delta q_{\text{O}} = -(\Delta q_1 + \Delta q_2), \quad (\text{S14})$$

with the neutrality fulfilled. Then, using q_{H}^0 and combinations (S12)-(S14), it is straightforward to recover the charges q_k necessary for computing the dipole $\boldsymbol{\mu}_i^0$ (S9).

Polarizability model. The polarizability of water molecule was described by a bond polarizability model that represents polarizability tensor $\boldsymbol{\alpha}$ of molecule in Cartesian frame as the sum of bond polarizabilities

$$\boldsymbol{\alpha} = \sum_i \boldsymbol{\pi}_i, \quad (\text{S15})$$

where the bond polarizability tensor $\boldsymbol{\pi}_i$ of OH bond i ($i = 1, 2$) is given by

$$\boldsymbol{\pi}_i = \mathbf{U}_i \mathbf{p}_i \mathbf{U}_i^{-1}. \quad (\text{S16})$$

Table S1: Coefficients in eqns (S12), (S13) and (S18) (in au, rad⁻¹, rad⁻²) for describing the dependence of atomic charges and OH bond polarizability tensor components on the geometry of water molecule.

Dipole model parameters								
C ₁	C ₂	C ₃	C ₄	C ₅	C ₆	C ₇	C ₈	C ₉
-0.13583	0.01507	0.02879	0.12088	0.05638	-0.05557	-0.06824	0.01472	0.11277
Polarizability model parameters								
P ₁	P ₂	P ₃	P ₄	P ₅				
5.63841	7.24435	3.53273	1.00417	2.90802				
P ₆	P ₇	P ₈						
4.80441	1.69457	0.34341						
P ₉	P ₁₀	P ₁₁	P ₁₂					
4.62814	0.69777	0.64988	-2.22892					

In (S16), \mathbf{U}_i stands for a rotation matrix transforming the bond polarizability tensor \mathbf{p}_i in its principal coordinates to the tensor $\boldsymbol{\pi}_i$ in the Cartesian frame. The tensor \mathbf{p}_i has the following form

$$\mathbf{p}_i = \begin{pmatrix} p_{i,L} & & \\ 0 & p_{i,T1} & \\ 0 & 0 & p_{i,T2} \end{pmatrix}, \quad (\text{S17})$$

where the subscripts L , $T1$ and $T2$ denote the longitudinal and two transversal axes of the bond polarizability tensor, respectively; the longitudinal axis is directed along the OH bond and the first transversal axis is perpendicular to the molecular plane. Dependence of the three non-zero components of \mathbf{p}_i on the internal coordinates was described with the following functional forms

$$\begin{aligned} p_{i,L} &= P_1 + P_2\Delta R_i + P_3\Delta R_i^2 + P_4\Delta R_j + P_5\Delta R_i\Delta R_j \\ p_{i,T1} &= P_6 + P_7\Delta R_i + P_8\Delta\theta \\ p_{i,T2} &= P_9 + P_{10}\Delta R_i + P_{11}\Delta\theta + P_{12}\Delta R_i\Delta R_j. \end{aligned} \quad (\text{S18})$$

Model parameters and model performance. The coefficients in eqns (S12), (S13) and (S18) were derived by fitting model atomic charges and molecular polarizabilities to reference values obtained in quantum-chemical calculations. For this purpose, geometry of an isolated water molecule was randomly varied in the limits $R_{\text{OH}} = (R_{\text{OH}}^0 - 0.1 \text{ \AA}, R_{\text{OH}}^0 + 0.2 \text{ \AA})$ and $\theta = (\theta_0 - 6^\circ, \theta_0 + 12^\circ)$ and ESP atomic charges and molecular polarizabilities were computed for a total of 300 configurations. The calculations used Gaussian09 code and were performed at the DFT level with the B3LYP exchange-correlation functional and pVTZ basis set by Sadlej³ that has been specifically designed to reproduce molecular dipoles and polarizabilities. The equilibrium value of hydrogen charge is equal to $q_{\text{H}}^0 = 0.3277 |e|$.

Values of the coefficients obtained in the least squares fits are reported in Table S1. Figure S1 illustrates the performance of the dipole and polarizability models. The former perfectly mimics changes of molecular dipole upon variation of molecular geometry. The latter also gives a very good agreement between the fitted and reference values of four non-zero components of the polarizability tensor; the majority of absolute relative errors for the polarizability tensor elements is smaller than 0.5 %. It should be noted that alternative functional forms for the polarizability tensor elements (S18) were tested, but they did not result in a notable improvement of the fit quality. Judging on the results presented in Figure S1, the quality of the dipole model is comparable with that used in ref. 2, while the polarizability model yields a better agreement between the model and reference quantities than such a model developed in ref. 2 (cf. Fig. 1, ref. 2).

Assessment of the model performance for the spectral intensity calculations was done by computing the infrared absorption coefficient and Raman activity of the vibrational modes. The dipole and polarizability

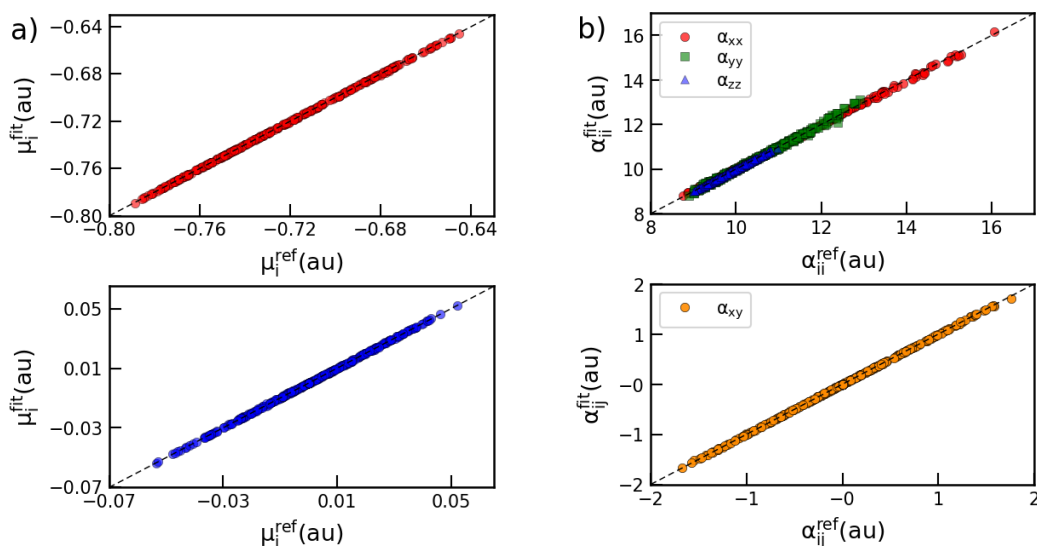


Figure S1: Correlations between the reference and model values of the non-zero dipole components (a), and of the non-zero elements of the polarizability tensor (b) in a total of 300 geometries of water molecule. Dashed line in the plots denotes the identity line.

tensor derivatives entering these quantities were obtained by the finite difference method using Cartesian vectors of atomic displacements in the vibrational modes. Figure S2 compares the spectral intensities yielded by the models with their counterparts obtained by the DFT calculations. The agreement is excellent in all cases, except the Raman activity of the angle-bending mode for which the polarizability model underestimates the activity by *ca.* 25 %. The reason for such a large error lies in the fact that the activity of the mode primarily comes from the anisotropy of the polarizability tensor derivative which has non-zero diagonal elements for this mode. As the anisotropy depends on difference between these elements, the relative error is amplified that, in its turn, causes a high relative error for this mode of low Raman activity.

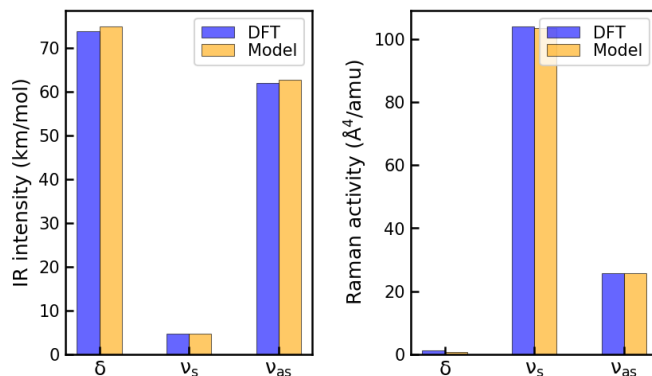


Figure S2: Comparison of infrared absorption coefficients (left) and Raman activities (right) of the vibrational modes of water molecule obtained in the DFT calculations and computed with the dipole and polarizability models; δ , ν_s and ν_{as} denote angle-bending, symmetric bond-stretching and asymmetric bond-stretching modes, respectively.

Finally, the models were tested by computing the dipole and polarizability variations in the vibrational modes of water molecule beyond the harmonic approximation. For this purpose, the atoms of H_2O molecule were displaced along the vectors of atomic displacements with large amplitudes. The variations of non-zero components of the dipole and polarizability tensor are compared with reference DFT values in Figure S3 and Figure S4 for the symmetric and asymmetric bond-stretching modes, respectively. The behaviour of the quantities is confidently reproduced at small and intermediate displacement amplitudes, but the agreement worsens when the amplitude increases. Nevertheless, the relative errors are small and the dipole and polarizability models have the quality sufficient for the purpose of the work.

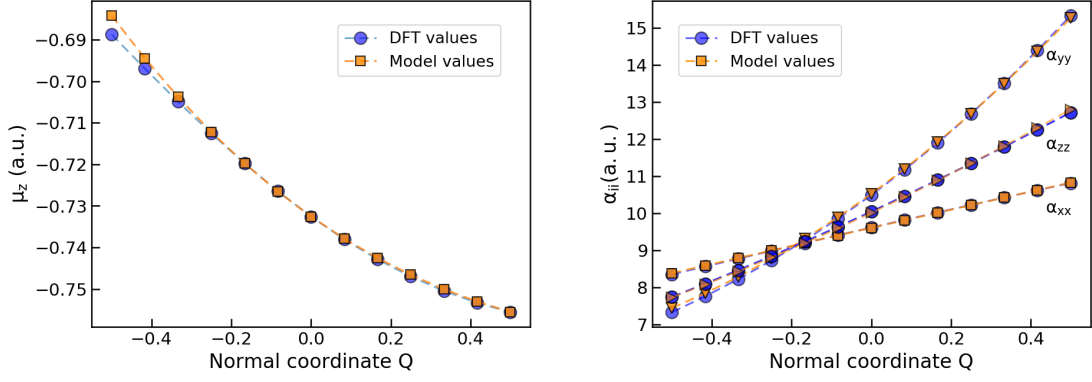


Figure S3: Variation of z-component of molecular dipole (left) and polarizability tensor elements (right) upon displacement of atoms of water molecule in the symmetric bond-stretching mode. The vector of Cartesian atomic displacements was multiplied by the factor Q shown along the x axis.

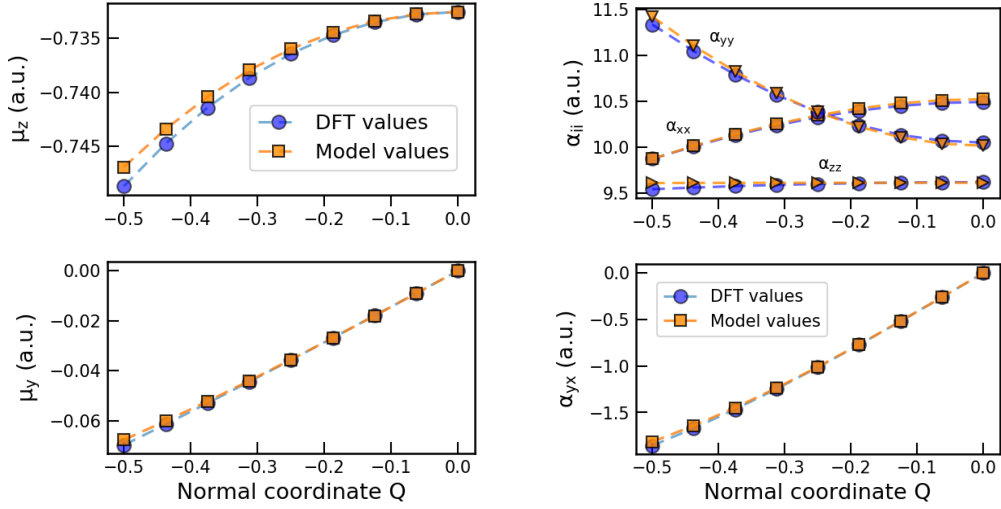


Figure S4: Variation of nonzero components of molecular dipole (left) and of polarizability tensor (right) upon displacement of atoms of water molecule in the asymmetric bond-stretching mode. The vector of Cartesian atomic displacements was multiplied by the factor Q shown along the x axis.

2 Second-order susceptibility calculations

The frequency-dependent $\chi^{(2),R}(\omega)$ tensor was computed using the time correlation function (TCF) formalism.^{2,4,5} According to the approach, the pqr element of $\chi^{(2)}(\omega)$ is given by

$$\chi_{pqr}^{(2),R}(\omega) = \frac{i\omega}{k_B T} \int_0^\infty dt e^{i\omega t} \langle M_r(0) \cdot A_{pq}(t) \rangle, \quad (\text{S19})$$

where M_r and A_{pq} stand for the r and pq components of the system dipole \mathbf{M} and polarizability \mathbf{A} , respectively, and k_B is the Boltzmann constant. Making use of (S1) and (S2), the time correlation function in (S19) for the $\chi_{ssp}^{(2),R}$ element reads

$$C_{ssp}(t) \equiv \langle M_p(0) \cdot A_{ss}(t) \rangle = \left\langle \sum_i \mu_{p,i}(0) \cdot \sum_j a_{ss,j}(t) \right\rangle. \quad (\text{S20})$$

For a slab of water molecules with the surface plane coinciding with the xy plane and the z -axis perpendicular to the the surface, the ssp element corresponds by the $\chi_{xxz}^{(2)}$ and $\chi_{yyz}^{(2)}$ components and (S20) can be recast to⁶⁻⁸

$$C_{ssp}(t) = \left\langle \sum_i \mu_{z,i}(0) \cdot [a_{xx,i}(t) + a_{yy,i}(t)] \right\rangle + \left\langle \sum_i \mu_{z,i}(0) \cdot \sum_{j \neq i} [a_{xx,j}(t) + a_{yy,j}(t)] \right\rangle, \quad (\text{S21})$$

where the first and second terms in (S21) are intramolecular (self) and intermolecular (cross) parts of the full TCF $C_{ssp}(t)$, respectively. The calculation of the cross TCF in (S21) was performed for molecules j with a mean r_{ij} distance less than 5.5 Å (second minimum in the oxygen-oxygen radial distribution function in bulk liquid water). A contribution of molecules of bulk region to the TCFs (S21) was attenuated⁷⁻⁹ by multiplying the dipole $\mu_{z,i}(0)$ by a damping function $g(z_i)$

$$\mu'_{z,i}(0) = g(z_i(0))\mu_{z,i}(0), \quad (\text{S22})$$

with $z_i(0)$ being the z -coordinate of molecular center-of-mass at $t = 0$; $\mu'_{z,i}(0)$ replaces $\mu_{z,i}(0)$ in (S21). The damping function $g(z)$ has the following form

$$g(z) = \frac{1}{2} \text{sign}(z) (\tanh(s(|z| - z_0)) + 1), \quad (\text{S23})$$

where $g(z_0) = 1/2$ and parameter s determines the width of transition region. Thus, $s = 2.1972 \text{ \AA}^{-1}$ gives the width of 1 Å for the 0.1 – 0.9 region. The $\text{sign}()$ function avoids the cancellation of the dipole M_z because of the symmetry of water slab with respect to $z = 0$. By changing z_0 , one can select a thickness of interfacial region for the computation of the $\chi_{ssp}^{(2),R}$ susceptibility.

The TCFs were computed on the length $N_c = 2048$ and multiplied by a Hann apodization function of width $N_c/2$ prior to performing the Laplace transform in (S19).

3 Characteristics of silica–water interface with QNULL and QESP parameter sets

Density and orientational order parameter profiles. Figure S5 displays the z -profiles of the relative density ρ^* and of the orientational order parameters S_2 (eqn. (3), main article) computed for the QNULL and QESP surfaces. It is noteworthy that the $S_2(z)$ profiles for the QESP set show an intermediate pattern between the profiles obtained with the QNULL and CLAYFF sets.

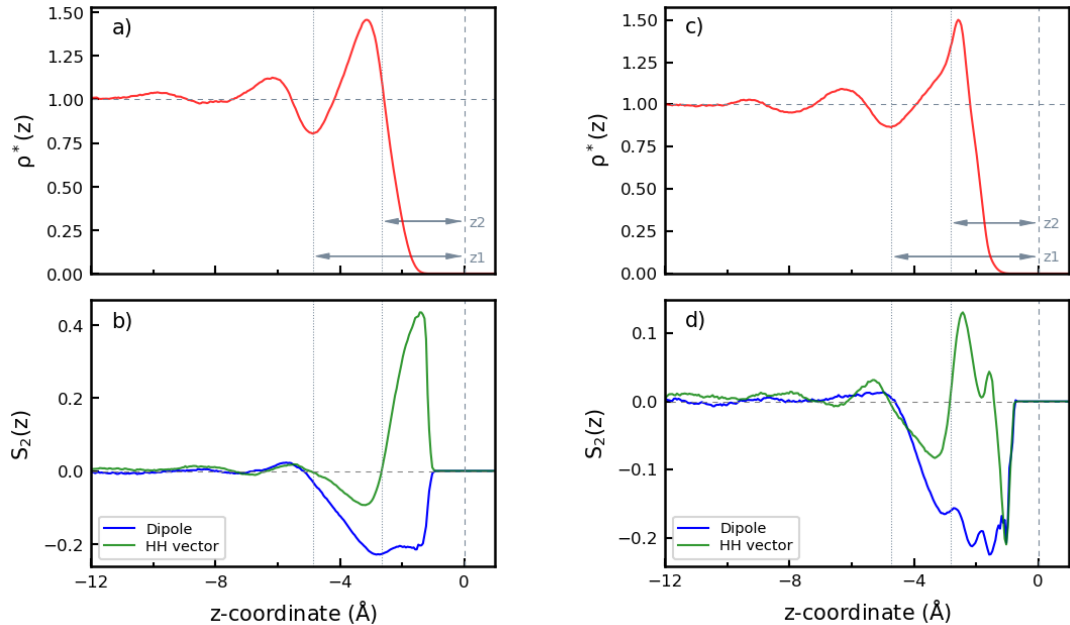


Figure S5: z -profiles of the relative density $\rho^* = \rho/\rho_0$ and of the orientational order parameters $S_2(z)$ of water molecules near the QNULL surface (panels a, b) and QESP surface (panels c, d). The vertical dashed line at $z = 0$ denotes the coordinate of the bottommost silica oxygen atoms taken as the origin of the z -axis; the horizontal dashed line indicates property value characteristic of bulk liquid water. Vertical dotted lines and the corresponding arrows labeled $z1$ and $z2$ are discussed in the text.

Probability density in the surface plane. Figure S6 shows the 2D probability density maps in the xy plane for water molecules in the z_2 region near the QNULL and QESP surfaces (Fig. S5). Note a marked increase of the probability density in the sites A (Fig. 6, main article) with the increase of charges of silica atoms from the QNULL ($q_{\text{Si}} = 0 |e|$) to QESP ($q_{\text{Si}} = 1.38 |e|$) sets.

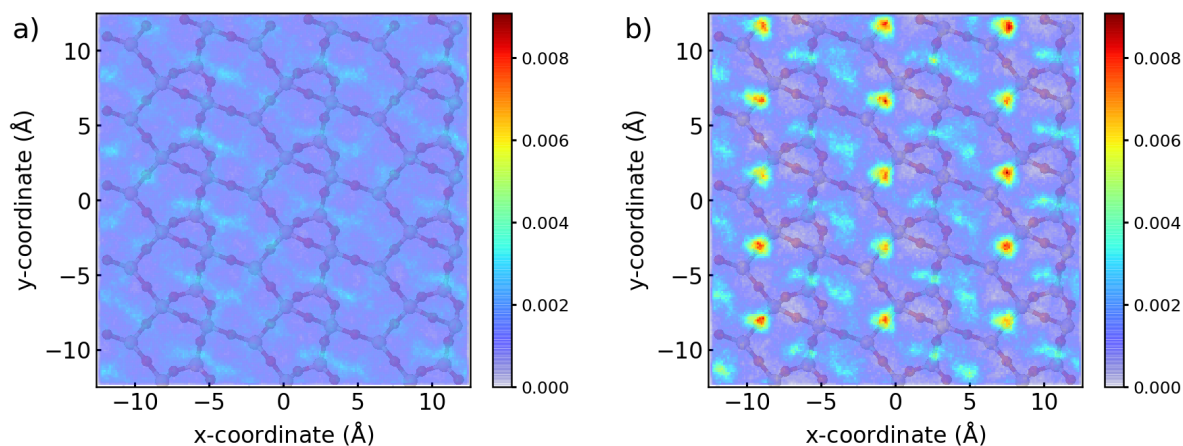


Figure S6: Maps of probability density (in \AA^{-2}) for water molecules in the plane parallel to the surface in the z_2 region; a) – QNULL parameters set, b) – QESP parameters set; the same intensity scale is used for the maps in the panels.

OH bonds orientation.

The probability density maps for the angles ψ between the OH vectors and the z -axis for water molecules near the QNULL and QESP surfaces are displayed in Figure S7.

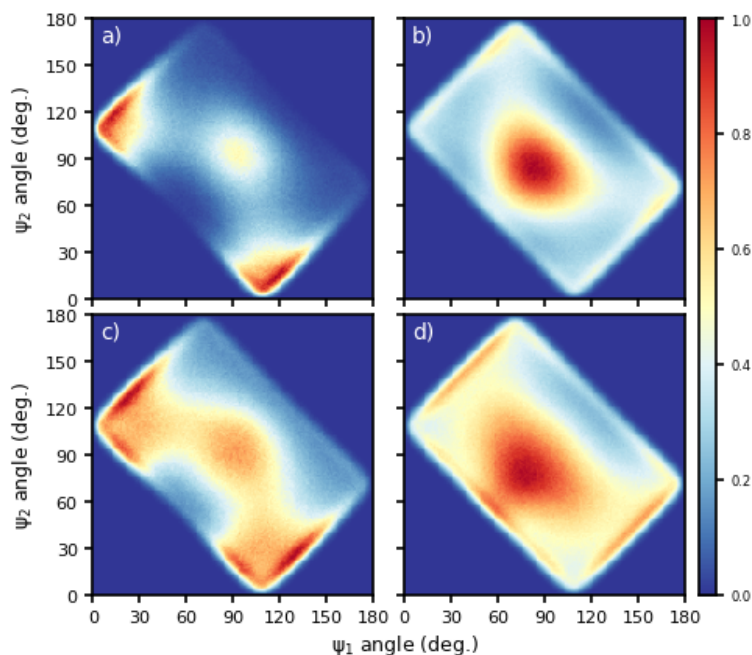


Figure S7: Two-dimensional probability density maps (in arb. units) of the angles ψ between the OH bonds and the z -axis for water molecules near the QNULL (a, b) and QESP (c, d) surfaces. Panels a, c – region z_2 ; panels b, d – region z_1 , see Fig. S5.

Sum-frequency generation spectra.

Figure S8 presents the $\text{Im}[\chi_{ssp}^{(2),R}]$ spectra computed for water on the QNULL and QESP surfaces and compares the spectra with the spectrum of water–vapor interface. Note a very similar appearance of the spectra for the

QNULL and water–vapor interfaces with a small downward shift due to weak van der Waals surface–water interactions.

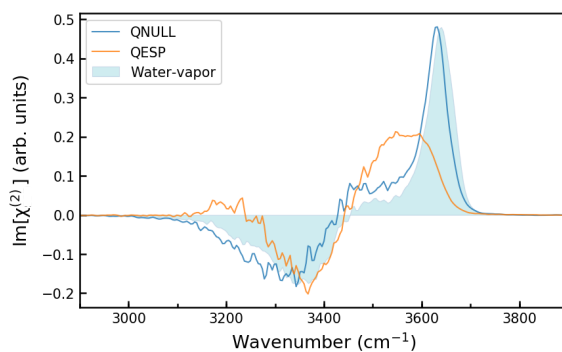


Figure S8: Spectrum of $\text{Im}[\chi^{(2),R}]$ for the QNULL and QESP silica–water interfaces; the spectrum for water–vapor interface is given for comparison as a filled shape.

Figure S9 displays the dependence of the spectra on the thickness of z -region taken in the calculation of the SFG spectra (parameter z_0 damping function (S23)). For both the hydrophobic surfaces the spectrum of the entire interfacial water is, to a large degree, determined by molecules in the $z1$ -region, the first water layer.

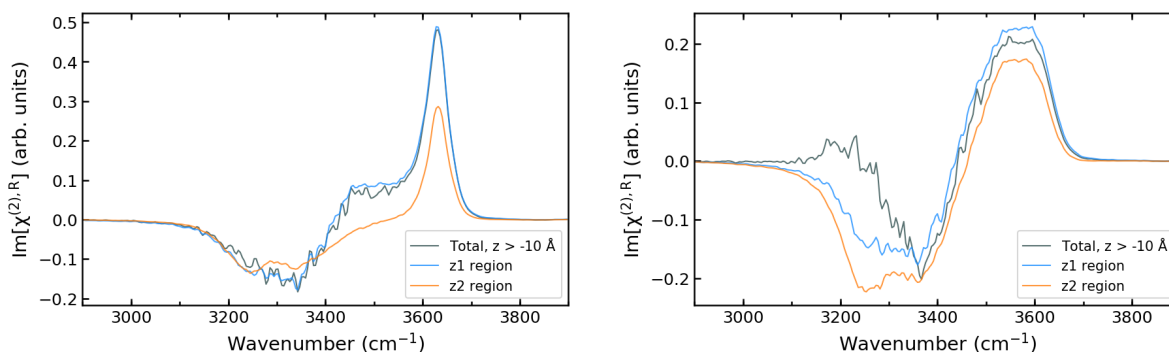


Figure S9: Spectra of $\text{Im}[\chi^{(2),R}]$ as a function of the distance z from the surface, see Figure S5 for the region definition; left – QNULL surface, right – QESP surface.

4 Water–vapor interface

Results of calculations for the water–vapor interface are reported for the sake of completeness. The simulated system consisted of 500 SPCFw molecules in a slab geometry with the size of the MD simulation box of 25.54 Å along the x and y directions. The calculations were carried out using the same computational protocol as for the interfacial systems (see Section 2.3, main article). Parameters of the damping function (S23) in the SFG spectra calculations were equal $z_0 = 8.0$ and $s = 2.1972 \text{ \AA}^{-1}$.

Density and orientational order parameter profiles.

The calculated $\rho^*(z)$ density profile and the profiles of the orientational order parameters S_2 are shown in Figure S10. The non-zero values of $S_2(z)$ for $z > 4 \text{ \AA}$ results from a few molecules escaped the water surface in the course of the simulations.

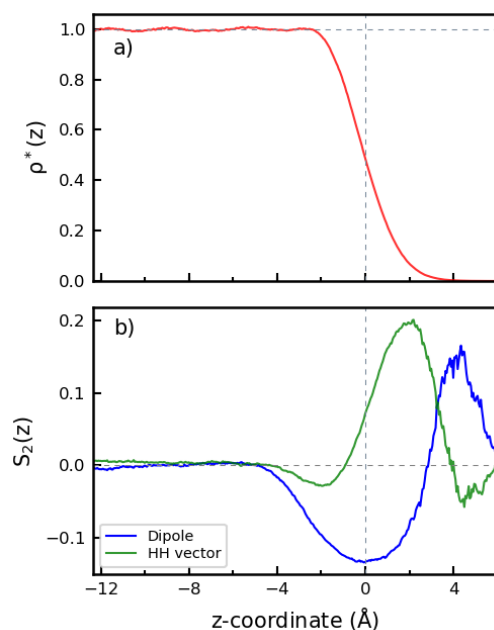


Figure S10: z-profiles of the relative density $\rho^* = \rho/\rho_0$ (a) and of the orientational order parameters $S_2(z)$ (b) of water–vapor interface. The vertical dashed line at $z = 0$ denotes the Gibbs dividing surface; the bulk water side and vapor side are situated in the regions with the negative and positive z values, respectively. The horizontal dashed line indicates property value characteristic of bulk liquid water.

Figure S11 presents the calculated spectra of the imaginary and real parts of the $\chi_{ssp}^{(2),R}$ susceptibility. The spectra are in a good agreement with the results obtained using essentially the same models for the dipole and polarizability of water molecule.⁹

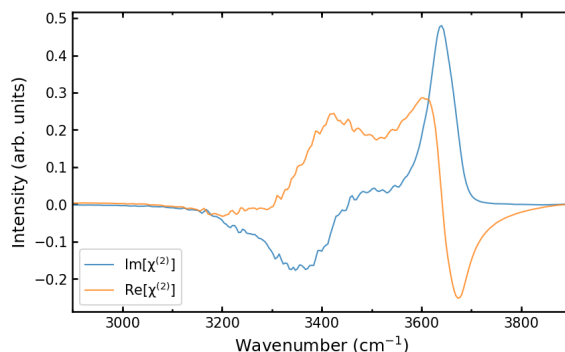


Figure S11: Calculated spectra of the imaginary and real parts of the $\chi^{(2),R}$ nonlinear susceptibility of water–vapor interface.

References

- [1] J. Applequist, J. R. Carl and K.-K. Fung, *J. Am. Chem. Soc.*, 1972, **94**, 2952–2960.
- [2] A. Morita and J. T. Hynes, *J. Phys. Chem. B*, 2002, **106**, 673–685.
- [3] A. J. Sadlej, *Collect. Czech. Chem. Commun.*, 1988, **53**, 1995–2016.
- [4] A. Perry, H. Ahlborn, B. Space and P. B. Moore, *J. Chem. Phys.*, 2003, **118**, 8411–8419.
- [5] A. Perry, C. Neipert, C. R. Kasprzyk, T. Green, B. Space and P. B. Moore, *J. Chem. Phys.*, 2005, **123**, 144705.
- [6] T. Ishiyama and A. Morita, *Chem. Phys. Lett.*, 2006, **431**, 78 – 82.
- [7] T. Ishiyama and A. Morita, *J. Phys. Chem. C*, 2007, **111**, 738–748.
- [8] Y. Nagata and S. Mukamel, *J. Am. Chem. Soc.*, 2011, **133**, 3276–3279.
- [9] A. Morita, *J. Phys. Chem. B*, 2006, **110**, 3158–3163.